Retrieved Vertical Profiles of Latent Heat Release Using TRMM Rainfall Products

W.-K. Tao[1], S. Lang[2], W. S. Olson[3], R. Meneghini[4], S. Yang[3], J. Simpson[1], C. Kummerow[1] and E. Smith[5]

[1]*Laboratory for Atmospheres*
[2]*Science Systems and Applications Inc.*
[3]*JCET/U. of Maryland Baltimore County*
[4]*Laboratory for Hydrospheric Processes*

NASA/Goddard Space Flight Center
Greenbelt, MD 20771

[5]*NASA/Marshall Space Flight Center*

Journal of Applied Meteorology

(January 27, 2000)

Corresponding author address: Dr. Wei-Kuo Tao, Mesoscale Atmospheric Processes Branch, Code 912, NASA/GSFC, Greenbelt, MD 20771
email: tao@agnes.gsfc.nasa.gov

Abstract

This paper represents the first attempt to use TRMM rainfall information to estimate the four dimensional latent heating structure over the global tropics for February 1998. The mean latent heating profiles over six oceanic regions (TOGA COARE IFA, Central Pacific, S. Pacific Convergence Zone, East Pacific, Indian Ocean and Atlantic Ocean) and three continental regions (S. America, Central Africa and Australia) are estimated and studied. The heating profiles obtained from the results of diagnostic budget studies over a broad range of geographic locations are used to provide comparisons and indirect validation for the heating algorithm estimated heating profiles.

Three different latent heating algorithms, the Goddard Convective-Stratiform (CSH) heating, the Goddard Profiling (GPROF) heating, and the Hydrometeor heating (HH) are used and their results are intercompared. The horizontal distribution or patterns of latent heat release from the three different heating retrieval methods are quite similar. They all can identify the areas of major convective activity (i.e., a well defined ITCZ in the Pacific, a distinct SPCZ) in the global tropics. The magnitude of their estimated latent heating release is also not in bad agreement with each other and with those determined from diagnostic budget studies. However, the major difference among these three heating retrieval algorithms is the altitude of the maximum heating level. The CSH algorithm estimated heating profiles only show one maximum heating level, and the level varies between convective activity from various geographic locations. These features are in good agreement with diagnostic budget studies. By contrast, two maximum heating levels were found using the GPROF heating and HH algorithms. The latent heating profiles estimated from all three methods can not show cooling between active convective events.

We also examined the impact of different TMI and PR rainfall information on latent heating structures. The rainfall estimated from the PR is smaller than that estimated from the TMI in the Pacific and Indian Oceans and the SPCZ causing weaker latent heat release in the CSH algorithm estimated heating using the PR derived rainfall information. In addition, the larger stratiform amounts

derived from the PR over S. America and Australia consequently lead to higher maximum heating levels. Sensitivity tests addressing the appropriate selection of latent heating profiles from the CSH look-up table were performed.

1. Introduction

The global hydrological cycle is central to climate system interactions and the key to understanding their behavior. Rainfall and its associated precipitation processes are a key link in the hydrologic cycle. Fresh water provided by tropical rainfall and its variability can exert a large impact upon the structure of the upper ocean layer. In addition, almost two-thirds of the global rain falls in the tropics, while the associated latent heat release accounts for three-fourths of the total heat energy for the Earth's atmosphere. Precipitation from convective cloud systems comprises a large portion of tropical heating and rainfall. Furthermore, the vertical distribution of convective latent-heat release modulates large-scale tropical circulations (e.g., the 30-60-day intraseasonal oscillation - see Sui and Lau, 1988), which, in turn, impact midlatitude weather through teleconnection patterns such as those associated with El Niño. Shifts in these global circulations can result in prolonged periods of droughts and floods, thereby exerting a tremendous impact upon the biosphere and human habitation. And yet, monthly rainfall over the tropical oceans was not known within a factor of two over large (5-degrees latitude by 5-degrees longitude) areas (Simpson *et al.* 1988, 1996). Hence the Tropical Rainfall Measuring Mission (TRMM), a joint U.S./Japan space project, is a critical mission. TRMM selected an inclined low-altitude orbit and a combination of precipitation radar, VIS/IR and microwave radiometers (see Simpson *et al.* 1996). It, therefore, will provide an adequate measurement of rainfall as well as estimate the four-dimensional structure of latent heating over the global tropics. The distributions of rainfall and inferred heating can be used to advance our understanding of the global energy and water cycle. In addition, this information can be used for global circulation and climate models for testing and improving their parameterizations.

Three types of latent heating profile retrievals have been developed for TRMM. The first algorithm estimates the latent heating profiles of clouds/cloud systems as a function of the vertical derivative of their retrieved hydrometeor profiles [termed a *hydrometeor/heating (HH)* algorithm - Tao *et al.* 1990 and Yang and Smith, 1999a and b]. The derivation and evaluation of the HH algorithm was based on cloud resolving model (CRM) simulations, and it requires information

about the vertical profiles of cloud- and precipitation-sized water and ice particles, all of which can be obtained from the TMI profiler retrievals (Kummerow *et al.* 1996; Smith *et al.* 1992, 1994). The terminal (fall) velocities of the large cloud (precipitating) particles (rain, snow and graupel/hail) are also required for the HH algorithm. Empirical coefficients associated with the condensation of small liquid water droplets and deposition of small ice particles are needed in Tao *et al.* (1990), and these coefficients can be determined using the surface rain rates (Tao *et al.* 1993a). Cloud-scale velocity is needed in Yang and Smith (1999b), and it is obtained by applying a regression method (to a CRM simulated data base). The second method, *the Convective and Stratiform Heating (CSH) algorithm*, was developed, and it only needs information on surface precipitation rates, amount of stratiform rain, and the type and location of observed cloud systems (Tao *et al.* 1993a). A lookup table, however, is used containing stored convective and stratiform latent heating profiles, normalized by total surface rain rates, for various types of cloud systems in different geographic locations. These profiles are mostly obtained from CRM (Goddard Cumulus Ensemble, GCE, model) simulations. In the third type, CRM simulated hydrometeor/latent heating vertical profiles that have radiative characteristics consistent with a given set of multispectral microwave radiometric observations are composited to create (retrieve) a best estimate of the observed profiles (termed a *Goddard profile (GPROF) heating algorithm*, Olson *et al.* 1999). Table 1 summarizes the cases and information needed in the previous latent heating retrieval studies.

During the TRMM mission, rainfall maps, stratiform amounts and vertical structure of hydrometeors are generated from TRMM algorithms. Products from the TRMM Microwave Imager (TMI) and from the Precipitation Radar (PR) can be used as input for the latent heating algorithms. The major objective of this study is to produce and examine four dimensional latent heating structures for February 1998 using different TRMM rainfall products. In Section 2, we will briefly review three different heating algorithms and their previous performance. The source of rainfall information derived from TRMM sensors will be described in Section 3. Retrieved latent heating profiles in global and in various geographic locations will be examined and discussed in Section 4. The CSH algorithm retrieved latent

heating structures will be compared to those of Olson *et al.* (1999) and Song and Smith (1999a and b) in Section 5. Summary and future work will be presented in Section 6.

2. TRMM Heating Algorithms

2.1 Hydrometeor/heating (HH) algorithm

The hydrometeor/heating (HH) algorithm developed at the Florida State University is based on the assumptions that an explicit 3-dimensional cloud model can be used to provide the microphysical underpinnings for an inversion-based retrieval procedure, and that latent heating rates are proportional to the vertical derivatives of retrieved liquid-ice water mass fluxes. The algorithm is a fully physical inversion technique designed to accept any combination of polarized or un-polarized satellite or aircraft passive microwave measurements.

Yang and Smith (1999a) analyzed their retrieved latent heating profiles from SSM/I and Q_2 (apparent moisture sink) profiles calculated from sounding data over the TOGA COARE IFA area. They found that their latent heating profiles are generally in agreement with diagnosed Q_2 profiles except the retrieved latent heating has a secondary peak around 1 km. Yang and Smith (1999b) also retrieved time-space mean monthly latent heating from SSM/I for the 1992 annual cycle. Results indicated that the retrieved latent heating fields show many stationary and transient features that are consistent with studies concerning cloudiness, convection and rainfall. However, the double-peak features of retrieved latent heating, a dominant peak around 5 km and a smaller one around 1 km, are not in good agreement with other diagnosed heating structures (e.g., Yanai *et al.* 1973; Thompson *et al.* 1979; Johnson, 1984; Lin and Johnson, 1996).

Yang and Smith (2000) modify their latent heating retrieval method by developing a new way to estimate a mean terminal velocity for liquid-ice water hydrometeors at SSM/I footprint scales. The small low level peak in the latent heating profiles is eliminated in the new procedure. They compare the retrieved

latent heating profiles and their diagnostic Q^1_1-Q_2 structures for convective and stratiform conditions over the TOGA COARE IFA. Other published Q_1-Q_2 structures for similar conditions are also included. Results show that retrieved latent heating and diagnosed heating structure are similar for convective situations, however, the low troposphere latent heating is not in agreement with diagnosed heating profiles. These suggest that their latent heating retrieval method has difficulties separating convective and stratiform conditions.

2.2 *Goddard Profiling (GPROF) heating algorithm*

Olson *et al.* (1999) retrieved atmospheric latent heating distributions associated with cloud systems that occurred during the TOGA COARE and Hurricane Andrew (1992) using SSM/I observations. Their estimation of the latent heating in Hurricane Andrew showed an increase in upper-level heating (near the inner core) as Andrew intensified. No (direct or indirect) observational data are available for validation in Andrew. However, this relationship between latent heating and intensification has been noted in studies by Rodgers *et al.* (1994) and Halverson *et al.* (1999). Olson *et al.*'s (1999) retrieved latent heating profiles for the TOGA COARE IFA show a low bias in the altitude of the maximum heating as well as excessive low-level cooling compared to rawinsonde-derived profiles.

The method of Olson *et al.* (1999) has been modified and adapted to observations of the TRMM Microwave Imager (TMI). First, the method of Hong *et al.* (1999) for estimating the fractional coverage of convection within a footprint from TMI brightness temperature horizontal texture has been combined with a new method for inferring the convective fraction from TMI 85.5 GHz polarization data. This combined estimate of convective area fraction within a TMI footprint weights the texture- and polarization-based estimates using the expected error variance of each estimate. When radiative scattering is weak, the texture-based method has the greatest influence on the combined estimate, whereas in regions of strong radiative scattering, the polarization-based method prevails.

---

1 Q_1 represents the apparent heating source and it consists of two components, the latent heat release and the divergence of eddy heat fluxes. Please see Yanai *et al.* (1973) for details.

This combined estimate of convective fraction is used to constrain TMI-retrieved latent heating profiles from the Goddard Profiling Algorithm (GPROF); see Section 3.1. As shown by Olson *et al.* (1999), the estimated convective fraction has a significant impact on estimates of the latent heating profile, since convective and stratiform regions are associated with fairly distinct vertical heating structures.

2.3 *Convective and stratiform heating (CSH) algorithm*

Diagnostic budget studies (Houze, 1982; Johnson, 1984) have shown that the distribution of heating in the anvil region of tropical mesoscale cloud systems is considerably different from the vertical profile of heating in the convective region. Tao and Simpson (1989), McCumber *et al.* (1991), and Tao *et al.* (1991; 1993b) have also shown that the microphysical processes are quite different in the convective and stratiform regions for GCE model simulated GATE, TAMEX, EMEX and PRE-STORM mesoscale convective systems[2]. For example, evaporative cooling in the lower troposphere is dominant in the stratiform region in all simulated convective systems. On the other hand, condensation/deposition heating is dominant in the convective region in these convective systems. Based on these findings, a convective-stratiform heating algorithm, has been developed (Tao *et al.* 1993a). Figure 1 is a flow chart that shows the procedure for deriving a latent heating profile from the CSH algorithm as well as the HH and GPROF heating algorithms. There are many sets of normalized heating profiles, each set has a convective profile and a stratiform profile simulated by a cloud resolving model (or cumulus ensemble model). Each set represents different system organizations as well as various geographic locations. The CSH derived heating profile can be evaluated by comparing with those estimated at well designed field campaigns (i.e., GATE, TOGA COARE[3], AMEX[4], ABLE[5], and TRMM field programs). Inputs

---

2 GATE stands for GARP (Global Atmospheric Research Program) Atlantic Tropical Experiment, TAMEX for Taiwan Area Mesoscale Experiment, EMEX for Equatorial Mesoscale Experiment and PRE-STORM for Preliminary Regional Experiment for Storm Central.

3 TOGA COARE stands for Tropical Oceans Global Atmosphere (TOGA) - Coupled Ocean Atmosphere Response Experiment (COARE).

4 AMEX stands for Australian Monsoon Experiment.

5 ABLE stands for Amazon Boundary Layer Experiment.

for the CSH algorithm are from spaceborne (TMI, PR and SSM/I) algorithm derivations.

Vertical profiles of latent heat release and their retrieval using the CSH algorithm associated with three TOGA COARE convective active periods[6] are examined by Tao *et al.* (1999). The inputs for the CSH algorithm are SSM/I (synthetic TMI) and Radar (synthetic TRMM PR) derived rainfall and stratiform amount. The 2-D GCE model simulated surface rainfall and straiform amount are also used to assess the strengths and/or deficiencies of the CSH algorithm. The GCE model simulated rainfall, stratiform amount and latent heating profiles are in excellent agreement with those estimated by upper level soundings and large-scale analyses (Lin and Johnson, 1996). In addition, the typical convective and stratiform heating structures (Johnson, 1984; Houze, 1989, 1997) are well captured by the GCE model. These modeled convective and stratiform heating profiles are used to expand the set of heating profiles in the CSH's look-up table.

Temporal variability of CSH algorithm retrieved latent heating profiles using radar estimated rainfall and stratiform amount is in good agreement with that diagnostically determined for all three periods. However, less rainfall and a smaller stratiform percentage estimated by radar[7] resulted in weaker (underestimated) latent heating profiles and lower maximum latent heating levels compared to those determined diagnostically. Rainfall information from SSM/I can not retrieve individual convective events due to poor temporal sampling. Sensitivity testing (using the results from the GCE model simulations) has been performed and the results indicate that the SSM/I derived time averaged stratiform amount may be underestimated for December 19-27. A higher (lower) percentage of stratiform rain can imply a maximum heating rate at a higher (lower) altitude (Tao *et al.* 1993b). Time averaged heating profiles derived from SSM/I, however, are not in bad agreement with those derived by soundings for the December 10-17 and February 9-13 convective periods. The heating retrievals

---

6 Three episodes (Dec 11-17 1992; Dec 19-27 1992; and Feb 9-13 1993) containing intense convection associated with WWBs and SSCs that occurred over the IFA were studied.

7 Johnson and Ciesielski (1999) indicated that the ship radars were located within a relatively dry region of the IFA. The smaller rainfall estimated from the ship radars could also be caused by the specific Z-R relationship applied in the stratiform region in Short *et al.* (1997).

may be more accurate for longer time scales provided there is no bias in the sampling.

3 TRMM Rainfall Products

Daily 0.5° gridded rainfall and percentage of rainfall classified as convective from the TMI and SSM/I and PR, respectively, for February 1998 are produced by GPROF (Olson *et al.*, 1999) and by the TRMM PR algorithm (Meneghini *et al.*, 1999). This fine resolution rainfall product will be used as the input for the CSH algorithm. Monthly 5° latent heating structures will be derived/averaged from the fine resolution heating profiles. The vertical structure of hydrometeors can also be retrieved based on Smith *et al.* (1992, 1994). These hydrometeor profiles, then, can be used for retrieving vertical latent heating structures using the HH algorithm (Yang and Smith, 1999a and b).

3.1 Goddard Profiling Algorithm (GPROF)

The basis of the retrieval method is the estimated expected value or "Bayesian" technique described in Kummerow *et al.* (1996) and Olson *et al.* (1996; 1999). The retrieval method is supported by a large database of hydrometeor profiles which are generated using three-dimensional, numerical cloud-resolving models. Microwave radiances at the TMI frequencies/polarizations are simulated from the three-dimensional model fields using an Eddington radiative transfer method. Given a set of actual TMI observed radiances, the retrieved hydrometeor profile is calculated as a weighted mean of the model profiles: only those model profiles associated with radiances similar to the observed radiances are assigned significant weights. A detailed description of the retrieval method utilized in the present study may be found in Olson *et al.* (1999).

In principle, any geophysical parameters (including hydrometeor profiles) derived from the cloud-resolving model simulations can be retrieved, as long as there is sufficient signal in the TMI radiance observations to distinguish various magnitudes of the desired parameters. In current applications of the TMI retrieval method, surface rainfall rate is defined as the 10 km x 10 km area average rain rate at the lowest model level. The dimension of the averaging area (10 km)

corresponds to the resolution of the 37 GHz TMI channel. Since the horizontal resolution of the cloud model simulations is on the order of 1 km, there are roughly 100 gridpoint rain rates which contribute to the area-average. Convective rain fraction is defined by first classifying each model gridpoint as either convective or non-convective using the technique described in Tao *et al.* (1993b).

$$f_R \equiv \frac{\sum_{i,j} R_{ij}\,\delta_{ij}}{\sum_{i,j} R_{ij}} \quad , \tag{1}$$

where

$$\delta_{ij} \equiv \begin{cases} 0; & \text{non-convective gridpoint} \\ 1; & \text{convective gridpoint} \end{cases} . \tag{2}$$

Here, Rij is the rain rate associated with gridpoint ij, and the summation is over all gridpoints within a given 10 km x 10 km area.

Vertical latent heating profiles are similarly determined by averaging the individual gridpoint model-derived profiles over 10 km x 10 km areas; see Olson *et al.* (1999) for more details. In the present study, the 10 km x 10 km average surface rain rate, convective rain fraction, and latent heating profile are all retrieved from TMI observations using the GPROF algorithm.

3.2 *TRMM PR Rainfall Algorithm*

The TRMM Precipitation Radar (PR) operates at a frequency 13.8 GHz. This is a moderately attenuating frequency so that one of the major objectives of the PR algorithms is to estimate and correct for the path attenuation. Because the PR is a single-wavelength, single-polarization, non-Doppler radar, there are only a few methods available. These include the Hitschfeld-Bordan (HB) method (Hitschfeld, and Bordan, 1954), the surface reference technique or SRT (Meneghini *et al.*, 1983), a "hybrid" of these (Iguchi and Meneghini, 1994, Iguchi *et al.*, 1998), and the mirror-image technique (Liao *et al.*, 1999). The rain rate estimation algorithm (which in the TRMM nomenclature is called 2a-25) uses a hybrid of the Hitschfeld-Bordan method and the SRT to correct for attenuation and derive an estimate of

the range profile of the radar reflectivity factor, dBZ. The rain rate profile is then calculated from the dBZ profile and an appropriate Z-R relationship. The algorithm also includes surface clutter rejection and an attempt to correct for effects of non-uniform beamfilling.

The major sources of data to the algorithm are the measured radar reflectivity factors, dBZm, derived from the radar return power without attenuation correction, and an estimate of path attenuation via the surface reference technique (algorithm 2a-21) with an associated reliability or accuracy of this estimate. The algorithm first defines the processing region, using only the data between the rain top and the lowest height above the surface that is free from surface clutter. The bright-band height and the climatological freezing height are used to define the regions of liquid, solid, and mixed phase hydrometeors. The initial values of the k-Z and Z-R relations are defined accordingly.

The attenuation correction is based primarily on the SRT which assumes that the decrease in the apparent surface cross section is caused by the propagation loss in rain. The coefficient α in the $k = \alpha Z^{**b}$ relationship (where k is the attenuation coefficient in dB/km) is adjusted so that the path-integrated attenuation (PIA), estimated from the HB method, matches that obtained from the SRT. This "α-adjustment" method assumes that the discrepancy between the PIA estimates from the SRT and the HB can be attributed to an inappropriate choice of α, or equivalently, an inappropriate choice of the rain drop size distribution. There are other ways, however, to use the path attenuation information provided by the SRT either by adjusting the radar constant (Meneghini *et al.* 1983) or by using the SRT path attenuation as a final value in the solution to the HB equation (Awaka *et al.* 1998).

To avoid inaccuracies in the attenuation correction when the SRT is unreliable, a hybrid of the SRT and HB method is used (Iguchi and Meneghini, 1994, Iguchi *et al.*, 1998). Generally, when the rain rate is low, the path attenuation determined from the HB method is weighted more heavily than the SRT which tends to have a large relative error at these rain rates. When the rain rate is moderate or high, the SRT estimate of path attenuation is normally given more

weight than the HB method, thereby avoiding the instabilities that usually occur in the HB estimate when the path attenuation is large.

Convective-stratiform classification of the rain is based on a combination of the vertical and horizontal structure of the radar reflectivity field (Awaka *et al.* 1998). The vertical profile is checked for the presence of a bright-band (melting layer) by considering the behavior of the second derivative of the radar range profile. Unless the maximum dBZ exceeds a threshold, the presence of a well-defined bright-band is used to indicate stratiform rain. In cases where a clearly defined melting layer is absent, the horizontal rain structure is examined by means a modified version of an algorithm designed for the analysis of ground-based radar data (Steiner *et al.* 1995).

Statistics of the instantaneous, high-resolution rain rates are compiled on a monthly basis over 5^{o} x 5^{o} latitude-longitude grids. Near-surface rain rates and the rain rates at 80 altitude levels are stored according to rain type. The statistics include means, standard deviations and histograms of the rain rate, radar reflectivity factors, bright-band and storm heights.

4. Results

Verification of the retrieved global and regional latent heating profiles is not an easy task because of the lack of direct observations both temporally and spatially on the global and regional scales. The heating profiles obtained from the results of diagnostic studies over a broad range of geographic locations as well as different years (Yanai *et al.* 1973; Chen, 1980; Johnson, 1984, 1992; Frank and McBride, 1989; Houze, 1989; Greco *et al.* 1994; Lin and Johnson, 1996 and others) will be used to provide comparisons and indirect validation for this study.

4.1 Rainfall and Stratiform Amount

Figure 2(a) shows the monthly mean rainfall (mm/day) for February 1998 derived from TMI (GPROF), respectively. Rainfall over six oceanic regions (TOGA COARE IFA, Central Pacific, S. Pacific Convergence Zone, East Pacific, Indian Ocean and

Atlantic Ocean) and three continental regions (S. America, Central Africa and Australia) is shown in Fig. 3. Clearly, a well defined ITCZ (associated with heavy precipitation) is present in the central Pacific between the Equator and 5 ^{o}S. The ITCZ is located between the Equator and 5 ^{o}N over the East Pacific. Weak convective episodes were present over the South Pacific Convergence Zone (SPCZ). Note that heavy precipitation is not located in the TOGA COARE IFA region. A similar feature was found during the TOGA COARE in 1992 and 1993 periods. Over the Indian Ocean, the precipitation events extend from South-West to North-East indicating the start of a Monsoon event. Over the Atlantic Ocean, a more distinct ITCZ is present over the West Atlantic than the East Atlantic. The precipitation episodes (monthly) over the continental regions are somewhat different from those over oceans. Heavy precipitation over Africa and Australia is centered, respectively, at 10 ^{o}S and between 20 ^{o}S and 15 ^{o}S. Over South America, heavy precipitation events are spread over a relatively large area. PR derived monthly precipitation patterns are also quite similar to that of GPROF except for the region near 35 ^{o}N in the Pacific Ocean and in the Atlantic Ocean (Fig. 2(b)). Discussion[8] on rainfall distribution and intercomparisons between PR and GPROF is the current focus of the TMI and PR algorithm developers. Both TMI and PR rainfall products will be used for the CSH algorithm.

Table 2 shows the GPROF and PR algorithm derived rainfall and its stratiform percentage for nine (six over the tropical ocean and three over land) different geographic locations. Overall, PR derived rainfall is smaller than rainfall estimated by TMI for all nine geographic locations, especially, (40% and 23%, difference respectively) over the Central and East Pacific Ocean. Rainfall over the Atlantic Ocean is almost identical (less than a 1% difference) between the TMI and PR. The difference (less than 14%) in rainfall over continental regions is smaller than over the Pacific and Indian Oceans between PR and TMI. Note that both two sensors indicated that the heaviest rainfall was over the Central Pacific and the weakest over the Atlantic Ocean.

---

8 Varying the drop-size distributions as well as explicit modeling of melting in the cloud resolving model simulations supporting the GPROF algorithm could lead to a significant change in the estimated surface rain and its stratiform percentage. The Goddard cloud modeling and rainfall retrieval groups are working closely to resolve this issue.

It is known that stratiform rain amounts are typically about 40-50% in organized convective systems in the tropics (Houze, 1997) with lower stratiform amounts (~30%-40%) for continental convective systems (Rutledge and Houze, 1987; Johnson and Hamilton, 1988). Therefore, both TMI and PR estimated stratiform percentages associated with oceanic and continental convective systems are probably very reasonable. The results from Table 2 also indicated that the difference in TMI and PR estimated stratiform percentage over the oceans is smaller than over the land. Small differences (5-7%) in the stratiform percentage for the Tropical oceanic convection can assure retrieving similar levels (altitude) of maximum latent heating (Tao *et al.* 1993a). The difference in stratiform percentage over South America and Australia is quite large (19%). Note that stratiform percentages were lower over the Atlantic, South America and Africa than over the Pacific and Indian Oceans from both PR and GPROF rainfall estimates.

4.2 *Latent Heating Profiles in the CSH Look-Up Table*

Selecting the appropriate latent heating profiles from the CSH algorithm's look-up table for specific convective events is not a trivial problem. Of course, the best set of heating distributions would be based on numerical simulations or diagnostics (using upper air soundings during intensive field campaigns) of one or more "representative" events observed during the period of interest. Initial conditions required for the cloud resolving model simulations are accurate vertical distributions of temperature, water vapor and winds and can only be obtained from field campaigns. It is very expensive to have field campaigns (with a dense upper air sounding network) over various geographic locations and at different seasons, however.

Two different approaches for selecting the latent heating profiles in the look-up table are used to obtain distinct estimates of the latent heating profiles in this study. *In the first approach,* normalized heating profiles represent oceanic and continental regions that were obtained by averaging profiles from the lookup table based on the growing (but still limited) set of GCE model simulations and

diagnostic studies (Figs. 9, 14 and 15 in Tao *et al.* 1993a, and Fig. 15 in Tao *et al.* 1999). These profiles are from Gallus and Johnson (1991 - PRESTORM), Yanai *et al.* (1973; but was partitioned into convective and stratiform components by Johnson, 1984 - Marshall Islands), Houze, (1989 - GATE), Houze and Rappaport (1984 - GATE), Chong and Hauser (1990 - Africa), Caniaux *et al.* (1993 - Africa), Tao and Simpson (1989 - GATE), Tao *et al.* (1991 - TAMEX), Tao *et al.* (1993(b) - EMEX and PRESTORM) and Tao *et al.* (1999 - West Pacific Warm Pool region). *In the second approach*, the heating profiles from look-up table profiles based on geographic locations and months of interest [i.e., Pacific (including TOGA COARE December 1992 and February 1993), Atlantic, Africa, N. America, and TOGA COARE from February of 1993] are applied in the CSH algorithm.

The heating profiles (normalized with surface rainrate) shown in Fig. 4 have a characteristic shape for the convective and stratiform heating (e.g., Houze, 1982; 1997). These include maximum convective heating in the lower to middle troposphere, maximum stratiform (anvil) heating in the upper troposphere, and regions of stratiform cooling prevailing in the lower troposphere. Also, larger heating aloft in the stratiform region is associated with larger cooling in the lower troposphere. However, some notable differences do exist. ***First***, convective heating is much weaker than its stratiform heating aloft for the continental convective systems (i.e., Fig. 4(b)). On the other hand, the convective heating is as strong as the stratiform heating for the oceanic convective systems (Fig. 4(a)). Warm rain processes and stratiform rain are more prevalent in tropical oceanic convective systems than in continental ones which may be the reason for these differences in latent heating. ***Second***, the level separating the heating and cooling in the stratiform region (indicating the freezing or melting level) is higher for the oceanic convective systems than the continental systems. The difference may be caused by the difference in surface temperature and surface pressure between oceans and continents. ***Third***, the heating and cooling associated with the stratiform region during the TOGA COARE in February 1993 are stronger than in December 1992. This feature may be explained by the fact that the convective systems that occurred during February 1993 had more stratiform clouds than those from the December periods (see Lin and Johnson, 1996; Tao *et al.* 1999). In addition, stratiform cooling for the Atlantic (GATE), Australia and Africa are

relatively small. The cooling is quite strong near the surface for the African convective system due to a dry boundary layer (Caniaux *et al.* 1993). The latent heating profiles modeled by the GCE and determined kinematically[9] are quite different for the GATE convective system. The impact on the retrieved latent heating profiles will be assessed in the next section.

4.3 Gridded 0.5 x 0.5 degree Daily and Monthly Latent Heating Profiles

a. Horizontal Distribution of Latent Heat Release

Figure 5 shows monthly mean latent heating at three different altitudes (2, 5 and 8 km) over the global tropics from the CSH algorithm using latent heating profiles in the look-up table representing general tropical oceanic and land regions (the first approach). The horizontal distribution pattern of the CSH estimated latent heating structures is very similar to the pattern of surface rainfall (Fig. 2), especially at middle and upper levels. For example, a well defined ITCZ in the east and central Pacific and in the Atlantic Ocean, a distinguished S. Pacific Convergence Zone (SPCZ), and broad areas of precipitation events spread over the continental regions, are present. Also, stronger latent heat release (10 K/day or greater) in the middle and upper troposphere is always associated with heavier surface precipitation. Heating in the upper troposphere over the Pacific and Indian Oceans is much stronger than the heating over Africa, S. America and the Atlantic Ocean. A higher tropopause and warmer surface temperatures over the tropical ocean may be the reason for the higher level of maximum latent heating. Differential heating between land and ocean in the upper troposphere could generate strong horizontal gradients in the thermodynamic fields and interact with global circulation.

One interesting result from Fig. 2 is the relatively strong cooling (-1 to -2 K/day) at 2 km level over the (East, Central and South) Pacific and Indian Oceans but not over the continental regions (i.e., Africa and S. America). It is not an expected result because the moisture content is higher over oceans. Cooling by

---

9 The convective and stratiform heating profiles were derived using composite "kinematic and thermodynamic" fields from radar, upper air soundings and aircraft measured winds.

evaporation of raindrops in the lower troposphere should be stronger over dry areas. Several previous observational studies were performed to analyze the heating budget obtained from sounding networks over the Pacific warm pool region and the Amazon region. For example, Lin and Johnson (1996) found weak cooling at low levels, probably induced by mesoscale downdrafts or evaporation by shallow cumuli, in the mean heating profile over the TOGA COARE region for the month of February 1993. Greco *et al.* (1994) calculated latent heating profiles from the ABLE network. Their results indicated that the distribution of heating is quite similar to the studies of those of West African squall lines (Chong and Hauser, 1990). Peak heating occurs between 500 and 550 hPa (about 5-6 km). Their results did not exhibit low level diabatic cooling for the ABLE case. They suggested that the lowermost 2-3 km over the Amazon rain forest canopy is characterized by a strong diurnal cycle of evapotranspiration and upward convective fluxes of moisture producing very large mixing ratios (Fitzjarrald *et al.* 1990). Model results (Scala *et al.* 1991) also suggested that dry tropospheric air is not present for the production and maintenance of evaporatively cooled downdrafts. The high moisture content during the wet season in the lower troposphere of the Amazon Basin may prevent or severely limit cooling below cloud base. Thus, more low level cooling over the Pacific than over S. America as estimated by the CSH heating algorithm is, perhaps, reasonable.

The CSH algorithm estimated latent heating structure using the second approach (selecting the heating profiles from the look-up table based on geographic location and month of interest) is shown in Fig. 6. The latent heating profiles shown in Figs. 4(a) and 4(c-h) are selected[10]. Horizontal distributions and variations of latent heating structures (i.e., Pacific and Atlantic ITCZ, an SPCZ and relatively scattered organization in Africa and S. America) between Figs. 5 and 6 are quite similar. Areas of cooling over the Pacific and Indian Oceans heating over the continental regions at low levels are also presence in the retrieved latent heating structures using the second approach. However, there are some notable differences between Figs. 5 and 6. The latent heat release at the 2 km level is

---

10 The profiles shown in Fig. 4(d) were selected for the Atlantic region, Fig. 4(e) for the Central Pacific, East Pacific, and TOGA COARE IFA regions, Fig. 4(f) for Africa, Fig. 4(g) for S. America, Fig. 4(h) for Australia, and Fig. 4(a) for all other oceanic regions.

stronger and over a larger area in the S. American and Australian region with the second approach. In addition, the latent heat release at middle and upper levels is stronger over the TOGA COARE IFA and Central and East Pacific regions than that based on general oceanic and continental heating profiles from the CSH look-up table. These results are simply caused by the fact that the heating profiles selected from the CSH look-up table are quite different in the two approaches. For example, the latent heating profiles shown in Fig. 4(e) were selected for the Central and East Pacific for the second approach and are stronger than the oceanic heating profiles in the first approach shown in Fig. 4(a).

b. Temporal Variation of Latent Heating Profiles

Time (daily) series of latent heating profiles derived from the CSH algorithm for nine different geographic locations are shown in Fig. 7. The maximum latent heating level varies with time with various convective events over Australia and the TOGA COARE IFA area. For latent heating profiles retrieved over the Central, East and South Pacific Ocean, the Indian Ocean, South America, and Africa, there is an almost constant maximum heating level, however. As discussed in Tao *et al.* (1993a), one of the major characteristics of the CSH algorithm is that the level of maximum latent heating is mainly determined by the stratiform percentage. This implies that there was no significant temporal (daily) variation in stratiform rainfall in the convective activity.

Frank *et al.* (1996) analyzed latent heating profiles for the 120 days of the TOGA COARE intensive observation period using an enhanced network of rawinsonde stations. They examined the heating profiles over several arrays, including the IFA (about 7° by 5°), the outer sounding array (OSA) (15° by 15°) and the large-scale array (25° by 30°). The results showed an interesting feature that was remarkably similar (i.e., maximum heating near 400 hPa, about 8 km AGL) for all three arrays over 120 days. Lin and Johnson (1996) compared the mean latent heating from the IFA, OSA and Marshall Islands region (Yanai *et al.* 1973). They also found that the heating profiles over the Western Pacific, although from regions with distinctly different convective characteristics, are surprisingly similar to one another. The maximum heating also occurred around 400 hPa as

indicated by Frank *et al.* (1996). The CSH algorithm retrieved latent heating structures and their small temporal variation over the Pacific and the TOGA COARE IFA region are in good agreement with these diagnostic studies.

Over the TOGA COARE IFA, Central and East Pacific (Figs. 7(a), 7(b) and 7(i)), about 6-8 convective events with lifecycles from two to three days were identified The temporal variation of the convective events retrieved over the SPCZ and Indian Ocean is smoother than that for the TOGA COARE IFA and the Central and East Pacific. This may imply that there are not just a few major convective events that dominate the total rainfall in these regions compared to their counterparts over the TOGA COARE IFA and the Central and East Pacific Ocean. The temporal variation of latent heating profiles over S. America and Africa is not much different from that over oceans. The above interpretation needs to be taken with caution and may have major limitations because of poor sampling by the TMI. For example, diagnostic heating budgets over the TOGA COARE IFA analyzed by Lin and Johnson (1996, Fig. 10 shown in their paper) show more (10) convective events in February 1993 with shorter life times (between a half to two days) compared to the CSH algorithm estimates.

There are several notable differences between the CSH algorithm estimated temporal latent heating structure variation and that from diagnostic studies over the TOGA COARE region (Lin and Johnson, 1996), GATE (Chen, 1980) and AMEX (Frank and McBride, 1989). ***First***, there is no significant cooling between two adjacent convective events (diurnal variation). This is because the CSH algorithm is based on surface rainfall. If there is no surface rainfall (i.e., inactive convection or a suppressed period), the CSH algorithm will only produce zero heating but not cooling. ***Second***, there is no temporal variation in heating or cooling in the lower troposphere as seen during TOGA COARE and GATE. The above two problems are, perhaps, the major shortcomings of the current CSH algorithm. ***Third***, the AMEX convective systems show little variability over system lifetimes or from system to system based on budget studies. The CSH algorithm estimated latent heating structure over Australia (Fig. 7(h)) does show strong temporal variation (the maximum heating level changes from system to system).

c. Monthly Mean Latent Heating Profiles over Various Geographic Locations

Figure 8 shows the monthly (February, 1998) mean latent heating profiles derived from the CSH heating algorithm for various geographic locations. Both approaches for selecting the heating profiles from the look-up table (Fig. 5 and Fig. 6) are shown. Over the Central and East Pacific regions, the latent heating profiles are quite similar in terms of the maximum heating level (near 8 km) and low level cooling (about 1 degree per day). Over the TOGA COARE IFA region, the cooling at low levels is smaller than in the Central and East pacific regions. This is caused by a smaller stratiform amount (45%) over the TOGA COARE IFA compared to the Central and East Pacific (52-54%). Over the SPCZ, the heating/cooling below 3 km is very weak, but there is a strong heating aloft. In the Atlantic region, the maximum heating level is at a high altitude (6-7 km). Over tropical continental regions, the low level cooling is present as over the Pacific, but it is very weak (less than 0.2 degrees per day). In addition, the maximum heating level (around 6 to 7 km) is lower than over the Pacific and Indian Oceans. A higher maximum heating level for the Pacific and Indian Oceans compared to a relatively low one for Africa, S. America and the Atlantic Ocean is in good agreement with diagnostic budget studies. The higher tropopause and warmer surface temperatures over the tropical oceans as suggested by Thompson *et al.* (1979) and Johnson (1992) are the reasons for the higher level of maximum latent heating over the Pacific than over the Atlantic and Australia. Note that latent heating is weaker over the SPCZ and Indian and Atlantic Oceans than over the Pacific. This is because less surface rainfall is estimated by the TMI in those regions.

Comparing the latent heating profiles using the first and second approaches shows that the heating in the middle and upper troposphere and the cooling in the low levels is much stronger in the second approach than in the first approach for the Central Pacific, East Pacific and TOGA COARE IFA. On the other hand, relatively small differences in latent heating magnitude are seen in other geographic locations. Over Africa and Australia, the maximum latent heating level shifts to a lower level (about 5-6 km level) using the second approach. On the other hand, the maximum latent heating level is shifted to a higher level in the second approach for the S. American region. Over the Atlantic ocean, one of

the maximum latent heating levels is located at 3 km (another one is at middle levels) when the GCE model simulated heating profiles are selected from the CSH algorithm look-up table.

5. Comparison of Latent Heating Profiles Derived by Various Heating Retrieval Algorithms

a. Horizontal Distribution of Latent Heat Release

Monthly mean latent heating profiles at three different altitudes (2, 5 and 8 km) using the GPROF heating algorithm over the tropics are shown in Fig. 9. The global distribution patterns of latent heating are quite similar between GPROF and that estimated from the CSH algorithm. No significant cooling is estimated over tropical continental regions (Africa and S. America) by the CSH algorithm. However, there are several notable differences in the latent heating distributions between GPROF the CSH algorithm. Strong cooling occurs from the low to middle troposphere from 25-35 ^{o}N in the Pacific and Atlantic Oceans in the GPROF estimates. The area of strong cooling in the lower troposphere in the Central Pacific, East Pacific and TOGA COARE IFA regions is very small. Most low level cooling occurs over the SPCZ. Also, the heating at the 5 km level is as strong as at the 8 km level over the Central Pacific, East Pacific, and S. America. This implies that multiple maximum heating levels could occur in these regions. These differences between the GPROF heating and the CSH algorithm estimated latent heating structures are more than we expected because the GPROF heating algorithm used GCE model simulated latent heating profiles as the data base, and these heating profiles also represent the major data base for the CSH algorithm's look-up table. One possible difference is that the profiles stored in the CSH algorithm's look-up table represent a life cycle (typically over 2-4 h) of clouds/cloud systems. In the GPROF heating algorithm's data base, the latent heating profiles represent the instantaneous latent heating corresponding to the hydrometeors that match the TMI.

Figure 10 shows the monthly mean latent heating profiles using the Hydrometeor Heating (HH) algorithm. The overall latent heating distributions

estimated by the HH algorithm and the CSH algorithm are in good agreement with each other at the 5 and 8 km levels. The similarity between the GPROF heating algorithm and HH algorithm estimated latent heating between 30 ^{o}S and 30 ^{o}N in the middle and upper troposphere is quite remarkable. The multiple maximum heating levels as estimated by the GPROF heating algorithm may also be present in the HH algorithm estimates over the Central Pacific, the East Pacific, the Indian Ocean and S. America. One of the major differences between the HH algorithm's and the CSH and GPROF heating algorithms' estimated heating distributions is in the lower troposphere. The HH algorithm heating is much weaker over all three continental regions (Africa, Australia and S. America). The heating over the Pacific and Indian Oceans is also quite weak compared to the other two heating retrieval methods. Also note that there is no strong low-level cooling over the Pacific region as estimated by the other two methods. The heating shown at low and middle levels from 30-35 ^{o}N over the Pacific and Atlantic Oceans is not retrieved by either the CSH nor the GPROF heating algorithm.

b. Monthly Mean Latent Heating Profiles over Various Geographic Locations

Figure 11 shows the monthly (February, 1998) averaged latent heating profiles derived from three different heating retrieval algorithms[11] over various geographic locations. Also the CSH heating algorithm using PR rainfall information is also shown for comparison. The GPROF heating and HH algorithm estimated mean latent heating profiles over the TOGA COARE IFA, Central and East Pacific regions are in better agreement with each other than they are to the CSH algorithm estimated. The multiple maximum heating levels (one at 4 km and another at the 6 km level) are shown in the GPROF heating algorithm estimated latent heating profiles. The HH algorithm estimated heating profiles are almost constant between 4 and 8 km levels. By contrast, only one maximum heating level (at 8 km) is estimated by the CSH algorithm. Diagnostic budget studies (Nitta, 1972; Yanai *et al.* 1973; Thompson *et al.* 1979 ; Frank *et al.* 1996 and

---

11 The first approach of selecting the latent heating profiles from the CSH look-up table is used for comparison.

Lin and Johnson, 1996) all showed that there is one maximum heating level at 7-8 km. Another difference in the vertical latent heating profiles between the CSH algorithm and the other two methods occurs in the 3-5 km layer. An interesting result is that the HH algorithm estimated latent heating shows cooling at low levels even though the area of stronger cooling is not shown in Fig. 9. This implies that the HH algorithm estimated cooling is weaker but covers a larger area compared to the other two methods. The rainfall estimated from the PR is smaller than that estimated from the TMI (Table 2), and that is the reason for weaker latent release in the CSH algorithm estimated heating using the PR derived rainfall information. Similar stratiform amounts derived from both the PR and TMI lead to a single maximum heating level at 8 km in the CSH algorithm.

The CSH and HH algorithm estimated latent heating profiles at middle and upper levels are in very good agreement with each other over the SPCZ and Indian Ocean. The GPROF heating algorithm estimated latent heating profiles in these regions still show two maxima (at 4 and 6 km) and are both lower than the CSH and HH algorithm estimated maximum heating levels. The lower tropospheric cooling determined by the GPROF heating algorithm is quite strong compared to that estimated from the other two methods. The same difference occurs between the CSH algorithm and the other two methods' estimated latent heating profiles again in the 3-5 km layer for these two oceanic regions as for the Pacific region. The lack of diagnostic budget studies in the SPCZ and Indian Ocean makes it very difficult to evaluate the performance of the three heating algorithms, however.

The latent heating profiles estimated by the three different heating algorithms are in very good agreement with each other above the 4 km level. Low level cooling is estimated by both the GPROF and HH methods but not by the CSH method. A distinct single mid-level (about 4-5 km) maximum heating is seen in the mean heating profile determined by a diagnostic budget study in GATE (Thompson *et al.* 1979). None of three methods retrieve this feature. Frank (1978), however, showed that multiple heating peaks for GATE cloud clusters during various stages of their life cycle (as shown in Fig. 9 in Johnson, 1992).

The HH algorithm estimated latent heating profiles show two distinct maximum heating levels (4 and 6 km) in the S. American, African and Australian regions. The GPROF heating algorithm also estimates two maximum heating levels at about 3 and 6 km (less pronounced than the HH algorithm estimated though). The CSH algorithm only estimated a single maximum heating level at 7, 6 and 6.5 km, respectively, for Australia, Africa and S. America. A single maximum in heating was obtained in AMEX/Australia just above the freezing (500-600 mb) level (Frank and McBride, 1989) and in ABLE/S. America at 5-6 km (Greco *et al.* 1994). The heating estimated by both GPROF heating and the HH algorithm is also stronger than that estimated by the CSH method over these three continental regions. The maximum heating level differs between the CSH algorithm using TMI and PR rainfall information over these continental regions. This is because the stratiform rain amounts estimated by these two sensors are quite different over continental regions (Table 2).

Johnson (1992) and Greco *et al.* (1994) showed the apparent heat source Q1 normalized by the observed precipitation rate for several diagnostic budget studies namely the western Pacific region (Reed and Recker, 1971; Nitta, 1972; Yanai *et al.* 1973), Florida (Johnson, 1976), the eastern Atlantic GATE region (Thompson *et al.* 1979), the Amazon (Greco *et al.* 1994), west Africa (Chong and Hauser, 1990), and the Great Plains (Gallus and Johnson, 1991). All of the profiles represented the composite heating resulting from a number of convective events at various stages of their life cycles. The maximum heating varies from 4.5 K day^{-1}/1 cm day^{-1} (GATE) to almost 10 K day^{-1}/1 cm day^{-1} (West Africa). All of the estimated latent heating profiles for the three different methods fall within the range of 4 to 8 K day^{-1}/1 cm day^{-1} (Figs. 8 and 11 and Table 2).

6. Summary and Future Work

This paper represents the first attempt to use TRMM rainfall information to estimate the latent heating structure over the global tropics for February 1998. Three different latent heating algorithms, the Goddard Convective-Stratiform Heating (CSH), the Goddard Profiling Algorithm (GPROF) heating, and the Hydrometeor Heating (HH), that have been developed for remote sensing (i.e.,

TRMM) are used and their results are intercompared. The latent heating profiles over six oceanic regions (TOGA COARE IFA, Central Pacific, S. Pacific Convergence Zone, East Pacific, Indian Ocean and Atlantic Ocean) and three continental regions (S. America, Central Africa and Australia) are estimated and studied. Verification of the retrieved global and regional latent heating profiles is not an easy task because of the lack of direct and observations both temporally and spatially on the global and regional scales. The heating profiles obtained from the results of diagnostic studies over a broad range of geographic locations (Yanai *et al.* 1973; Johnson, 1984, 1992; Thompson *et al.* 1979; Houze, 1989; Frank and McBride, 1989; Greco *et al.* 1994; Frank *et al.* 1996; Lin and Johnson, 1996 and many others) are used to provide comparisons and indirect validation for the CSH algorithm, the HH algorithm and the GPROF heating algorithm estimated heating profiles.

Table 3 summarizes the major characteristics of the latent heating profiles/structures estimated from the three different heating retrieval algorithms as well as previous diagnostic budget studies. The horizontal distribution or patterns of latent heat release from the three different heating retrieval methods are quite similar. They all can identify the areas of major convective activity (i.e., a well defined ITCZ in the Pacific, a distinct SPCZ) in the global tropics. The magnitude of their estimated latent heating release is also not in bad agreement with each other. However, the major difference among these three heating retrieval algorithms is the altitude of the maximum heating level. The CSH algorithm estimated heating profiles show only one maximum heating level and the level varies between convective activity from various geographic locations. By contrast, two maximum heating levels were found using the GPROF heating and HH algorithms. The latent heating profiles estimated from all three methods can not show cooling between active convective events. The diurnal variation of latent heat structures at low levels seen from diagnostic budget studies in TOGA COARE can not be retrieved due to the poor sampling in TRMM.

Two different approaches for selecting the latent heating profiles in the CSH look-up table were used and tested. In the first approach, normalized heating profiles represent oceanic and continental regions that were obtained by averaging profiles from the lookup table based on the growing (but still limited) set of GCE

model simulations and diagnostic studies. In the second approach, the heating profiles from the look-up table are selected based on geographic locations and months of interest. The results showed that horizontal distributions and variations of latent heating structures (i.e., Pacific and Atlantic ITCZ, an SPCZ and relatively scattered organization in Africa and S. America) is not affected. Areas of cooling over the Pacific and Indian Oceans and heating over the continental regions at low levels are present in the retrieved latent heating structures using both approaches. Also, a single maximum heating level in all geographic locations is shown in both approaches. However, there are some notable differences in terms of magnitude (1 K day^{-1} in the low troposphere to 2-3 K day^{-1} in the middle to upper troposphere) of the latent heat release and the altitude (by 1-2 km) of maximum heating. Finding a systematic method to select an appropriate set of profiles from the look up table is an area that requires further investigation.

The rainfall estimated from the PR is smaller than that estimated from the TMI in the Pacific and Indian Oceans and the SPCZ causing weaker latent heat release in the CSH algorithm estimated heating using the PR derived rainfall information. Similar stratiform amounts derived from both the PR and TMI lead to a single maximum heating level at 8 km in the CSH algorithm over the tropical oceans. The larger stratiform amounts derived from the PR over S. America and Australia consequently lead to higher maximum heating levels.

Heating profiles for the TRMM Field Campaign sites (i.e., SCSMEX[12], May - June 1998; LBA[13] - TRMM/Brazil, January - February 1999; and KWAJEX[14], July - September 1999) as well as other major field campaigns such as DOE/ARM[15] will be produced and compared/evaluated for the three different heating algorithms using those determined from sounding networks. This future intercomparison can provide us with an assessment of the absolute and relative errors of these heating retrieval algorithms. In addition, global analyses will be used to

---

12 SCSMEX stands for South China Sea Monsoon Experiment.

13 LBA stands for Large Scale Biosphere-Atmosphere Experiment.

14 KWAJEX stands for The Kwajalein Experiment.

15 DOE/ARM stands for Department of Energy Atmospheric Radiation Measurement.

identify/compare the large-scale circulation patterns for the retrieved periods and for periods during previous field campaigns (i.e., TOGA COARE and GATE). It may be reasonable to assume that the latent heating structures for Westerly Wind Bursts (WWBs) and Super Cloud Clusters (SCCs) occurring in similar large-scale circulations and with similar SSTs could not be very different.

Four dimensional fields of latent heating from the Florida State University (FSU) global model at the resolution T170 will also be compared (personal communication - Prof. T. N. Krishnamurti). This intercomparison may provide information about the capabilities and deficiencies of the current moist processes represented in the FSU global model (as well as other GCMs and climate models). A regional (0.5^{o}) daily four dimensional latent heating structure can be produced over the lifetime of TRMM (November 1997 to the mission's end). The regional scale products will be averaged to generate a 5^{o} monthly latent heating profile product. Long term latent heating structures are needed to improve our understanding of the interaction between large-scale circulation and convectively generated latent heat release. In addition, the TRMM estimated four dimensional latent heating structures can be used as forcing in the theoretical studies of the intraseasonal oscillation and its relationship/interaction with ENSO onset (i.e., Sui and Lau, 1988).

7. Acknowledgments

This study is supported by the NASA Headquarters Physical Climate Program and by the NASA TRMM project. The authors are grateful to Dr. R. Kakar (NASA/HQ) for his support of this research. Acknowledgment is also made to NASA/Goddard Space Flight Center for computer time used in the research.

8. References

Awaka, J., T. Iguchi, and K. Okamoto, 1998: Early results on rain type classification by the Tropical Rainfall Measuring Mission (TRMM) precipitation radar, *Proc. 8th URSI Commission F Open Symp., Aveiro, Portugal,* 143-146.

Caniaux, G., J.-L. Redelsperger and J.-P. Lafore, 1993: A numerical study of the stratiform region of a fast-moving squall line. Part I: General description and water and heat budgets. *J. Atmos. Sci.*, (submitted).

Chen, Y.-L., 1980: The relationship between organized convective systems and large-scale fields observed in GATE. Ph. D. Thesis, Lab. for Atmos. Res., University of Illinois, Urbana, Il., 148pp.

Chong, M., and D. Hauser, 1990: A tropical squall line observed during the COPT 81 experiment in West Africa. Part III: Heat and moisture budgets. *Mon. Wea. Rev.*, **118**, 1696-1706.

Fitzjarrad, D. R., K. E. Moore, O. M. R. Cabral, J. Scala, A. O. Manzi and L. D. de Abreu, 1990: Daytime turbulent exchange between the Amazon forest and the atmosphere. *J. Geophys. Res.*, **95**, 16825-16838.

Frank, W. M., 1978: The life cycles of GATE convective systems. *J. Atmos. Sci.*, **35**, 1256-1264.

Frank, W. M., and J. L. M. Bride, 1989: The vertical distribution of heating in AMEX and GATE cloud clusters. *J. Atmos. Sci.*, **46**, 3464-3478.

Frank, W. M., H. Wang, and J. L. McBride, 1996: Rawinsonde budget analysis during the TOGA COARE IOP. *J. Atmos. Sci.*, **53**, 1761-1780.

Gallus, W. A., Jr. and R. H. Johnson, 1991: Heat and moisture budgets of an intense midlatitude squall line. *J. Atmos. Sci.*, **48**, 122-146.

Hitschfeld, W., and J. Bordan, 1954: Errors inherent in the radar measurement of rainfall at attenuating wavelengths. *J. Atmos. Sci.*, **11**, 58-67.

Hong, Y., C. D. Kummerow and W. S. Olson, 1999: Separation of convective and stratiform precipitation using microwave brightness temperature. *J. Applied Meteor.*, **38**, 1195-1213.

Houze, R. A., Jr., 1982: Cloud clusters and large-scale vertical motions in the tropics. *J. Meteor. Soc. Japan*, **60**, 396-409.

Houze, R. A., Jr., 1989: Observed structure of mesoscale convective systems and implications for large-scale heating. *Quart. J. Roy. Meteor. Soc.*, **115**, 425-461.

Houze, R. A., Jr., 1997: Stratiform precipitation in regions of convection: A meteorological paradox. *Bull. Amer. Meteor. Soc.*, **78**, 2179-2196.

Houze, R. A., Jr., and E. N. Rappaport, 1984: Air motions and precipitation structure of an early summer squall line over the eastern tropical Atlantic. *J. Atmos. Sci.*, **41**, 553-574.

Iguchi, T and R. Meneghini, 1994: Intercomparisons of single-frequency methods for retrieving a vertical rain profile from airborne or spaceborne radar data. *J. Atmos. Oceanic Technol.*, **11**, 1507-1516.

Iguchi, T., T. Kozu, R. Meneghini, J. Awaka, K. Okamoto, 1998: Preliminary results of rain profiling with TRMM Precipitation Radar, *Proc. Of URSI-F International Triennial Open Symposium on Wave Propagation and Remote Sens., Aveiro, Portugal*, 147-150.

Greco, S., J. Scala, J. Halverson, H. L. Massie, W.-K. Tao and M. Garstang, 1994: Amazon coastal squall lines. Part II: Heat and moisture transports. *Mon. Wea. Rev.*, **122**, 623-635.

Johnson, R. H., 1976: The role of convective-scale precipitation downdrafts in cumulus and synoptic scale interactions. *J. Atmos. Sci.*, **33**, 1890-1910.

Johnson, R. H., 1984: Partitioning tropical heat and moisture budgets into cumulus and mesoscale components: Implication for cumulus parameterization. *Mon. Wea. Rev.*, **112**, 1656-1665.

Johnson, R. H., 1992: Heat and moisture sources and sinks of Asian Monsoon precipitating systems. *J. Meteor. Soc. Japan*, **70**, 353-371.

Johnson, R. H., and P. J. Hamilton, 1988: The relationship of surface pressure features to the precipitation and airflow structure of an intense midlatitude squall line. *Mon. Wea. Rev.*, **116**, 1444-1471.

Kummerow, C., W. S. Olson, and L. Giglio, 1996: A simplified scheme for obtaining precipitation and vertical hydrometeor profiles from passive microwave sensors. *IEEE Trans. Geosci. Remote Sensing*, **34**, 1213-1232.

Kummerow, C., W. Barnes, T. Kozu, J. Shiue, and J. Simpson, 1998: The tropical rainfall measuring mission (TRMM) sensor package. *J. Atmos. Oceanic Tech.*, **15**, 809-817.

Liao, L., R. Meneghini, and T. Iguchi, 1999: Simulations of mirror image return of air/space-borne radar in rain and their applications in estimating path attenuation. *IEEE Trans. Geosci. and Remote Sens.*, **37**, 1107-1121.

Lin, X., and R. H. Johnson, 1996: Heating, moistening and rainfall over the western Pacific during TOGA COARE. *J. Atmos. Sci.*, **53**, 3367-3383.

McCumber, M., W.-K. Tao, J. Simpson, R. Penc, and S.-T. Soong, 1991: Comparison of ice-phase microphysical parameterization schemes using numerical simulations of tropical convection. *J. Appl. Meteor.*, **30**, 985-1004.

Meneghini, R., J. Eckerman, and D. Atlas, 1983: Determination of rain rate from a spaceborne radar using measurements of total attenuation. *IEEE Trans. Geosci. Remote Sens.*, **21**, 34-43.

Meneghini, R., T. Iguchi, T. Kozu, L. Liao, K. Okamoto, J. A. Jones and J. Kwiatkowski, 1999: Use of the surface reference technique for path attenuation estimates from TRMM radar. *J. Appl. Meteor.* (submitted).

Nitta, T., 1972: Energy budget of wave disturbances over the Marshall Islands during the years of 1956 and 1958. *J. Meteor. Soc. Japan*, **50**, 71-84.

Olson, W. S., C. D. Kummerow, G. M. Heymsfield, and L. Giglio, 1996: A method for combined passive-active microwave retrievals of cloud and precipitation profiles. *J. Appl. Meteor.*, **35**, 1763-1789.

Olson, W. S., C. D. Kummerow, Y. Hong, and W.-K. Tao, 1999: Atmospheric latent heating distributions in the Tropics derived from passive microwave radiometer measurements. *J. Appl. Meteor.*, **38**, 633-664.

Reed, R. J. and E. E. Recker, 1971: Structure and properties of synoptic-scale wave disturbances in the equatorial western Pacific. *J. Atmos. Sci.*, **28**, 1117-1133.

Rutledge, S. A., and R. A. Houze, Jr., 1987: A diagnostic modeling study of the trailing stratiform rain of a midlatitude squall line. *J. Atmos. Sci.*, **44**, 2640-2656.

Scala, J., M. Garstang, W.-K. Tao, K. Pickering, A. Thompson, J. Simpson, V. Kirchhoff, E. Browell, G. Sachse, A. Torres, G. Gregory, R. Rasmussen and M. Khalil, 1990: Cloud draft structure and trace gas transport. *J. Geophys. Res.*, **95**, 17015-17030.

Simpson, J., R. F. Adler, and G. R. North, 1988: A proposed satellite tropical rainfall measuring mission (TRMM). *Bull. Amer. Meteor. Soc.*, **69**, 278-295.

Simpson, J., C. Kummerow, W.-K. Tao and R. Adler, 1996: On the Tropical Rainfall Measuring Mission (TRMM) *Meteor, and Atmos. Phys.* 60, 19-36.

Smith, E. A., X. Xiang, A. Mugnai and G. J. Tripoli, 1992: A cloud-radiation model algorithm for spaceborne precipitation retrieval. Extended Abstract Vol. of *International TRMM Workshop on the Processing and Utilization of the*

Rainfall Data Measured from Space, Communications Research Laboratory, Tokyo, Japan, 273-283.

Smith, E. A., X. Xiang, A. Mugnai and G. J. Tripoli, 1994: Design of an inversion-based precipitation profile retrieval algorithm using an explicit cloud model for initial guess microphysics. *Meteor. Atmos. Phys.*, **54**, 53-78.

Steiner, M. R., R. A. Houze, Jr. and S. E. Yuter, 1995: Climatological characterization of three-dimensional storm structure from operational radar and rain gauge data. *J. Appl. Meteor.*, **34**, 1978-2007.

Sui, C.-H., and K.-M. Lau, 1989: Origin of low-frequency (Intraseasonal) oscillations in the tropical atmosphere. Part II: Structure and propagation of mobile wave-CISK modes and their modification by lower boundary forcings. *J. Atmos. Sci.*, **46**, 37-56.

Tao, W.-K., and J. Simpson, 1989: Modeling study of a tropical squall-type convective line. *J. Atmos. Sci.*, **46**, 177-202.

Tao, W.-K., J. Simpson, S. Lang, M. McCumber, R. Adler and R. Penc, 1990: An algorithm to estimate the heating budget from vertical hydrometeor profiles. *J. Appl. Meteor.*, **29**, 1232-1244.

Tao, W.-K., J. Simpson and S.-T. Soong, 1991: Numerical simulation of a subtropical squall line over Taiwan Strait. *Mon. Wea. Rev.*, **119**, 2699-2723.

Tao, W.-K., S. Lang, J. Simpson and R. Adler, 1993a: Retrieval Algorithms for estimating the vertical profiles of latent heat release: Their applications for TRMM. *J. Meteor. Soc. Japan* , **71**, 685-700.

Tao, W.-K., J. Simpson, C.-H. Sui, B. Ferrier, S. Lang, J. Scala, M.-D. Chou and K. Pickering, 1993b: Heating, moisture and water budgets of tropical and midlatitude squall lines: Comparisons and sensitivity to longwave radiation. *J. Atmos. Sci.*, **55**, 673-690.

Tao, W.-K, S. Lang, J. Simpson, W. Olson, D. Johnson, B. Ferrier, C. Kummerow, D. Short and R. Adler, 1999: Vertical profiles of latent heat release and their retrieval in TOGA COARE convective systems using a cloud resolving model, SSM/I and radar data. *J. Meteor. Soc. Japan*, (accepted).

Thompson, R. M., Jr., S. W. Payne, E. E. Recker, and R. J. Reed, 1979: Structure and properties of synoptic-scale wave disturbances in the intertropical convergence zone of the eastern Atlantic. *J. Atmos. Sci.*, **36**, 53-72.

Yanai, M., S. Esbensen and J. Chu, 1973: Determination of average bulk properties

of tropical cloud clusters from large-scale heat and moisture budgets *J. Atmos. Sci.*, **30**, 611-627.

Yang, S., and E. A. Smith, 1999a: Moisture budget analysis of TOGA-COARE area using SSM/I retrieved latent heating and large scale Q_2 estimates. *J. Atmospheric and Oceanic Technology*, **16**, 633-655.

Yang, S., and E. A. Smith, 1999b: Four Dimensional structure of monthly latent heating derived from SSM/I satellite measurements. *J. Climate*, **12**, 1016-1037.

Yang, S., and E. A. Smith, 2000: Vertical structure and transient behavior of convective-stratiform heating in TOGA-COARE from combined satellite-sounding analysis. *Journal of Applied Meteorology* , in press.

FIGURE CAPTIONS

Fig. 1 Diagram showing the procedure for deriving a latent heating profile using the Convective-Stratiform Heating (CSH), HH and GPROF heating algorithm. Various rainfall products needed for these three different heating algorithms are shown. The heating profiles in the look-up table are from diagnostic and CRM-simulated convective and stratiform heating profiles for various geographic locations.

Fig. 2 Monthly mean rainfall (mm/day) for February 1998 derived by **(a)** the GPROF and **(b)** the PR. The rainfall and its stratiform amount as well as the latent heating profiles will be compared and examined for the various geographic locations identified by the boxes.

Fig. 3 Monthly mean rainfall (mm/day) for February 1998 for various geographic locations. The geographic areas are **(a)** the Central Pacific, **(b)** the East Pacific, **(c)** the South Pacific Convergence Zone, **(d)** the Indian Ocean, **(e)** the Atlantic Ocean, **(f)** South America, **(g)** Africa, **(h)** Australia, and **(i)** the TOGA COARE IFA region.

Fig. 4 The convective/stratiform heating profiles stored in the heating profile look-up table for the CSH algorithm. The profiles represent **(a)** tropical oceans, **(b)** general land areas, **(c)** the Pacific warm pool region, **(d)** the East Atlantic region (GATE - both total averaged and GCE simulated), **(e)** the TOGA COARE for February 1993, **(f)** Africa (COPT-81), **(g)** midlatitude USA (PRESTORM), and **(h)** Australia (EMEX).

Fig. 5 Monthly mean latent heating profiles at **(a)** 8, **(b)** 5 and **(c)** 2 km over the global tropics. Latent heating profiles representing just tropical oceanic and general land regions from CSH look-up table (LUT) were used.

Fig. 6 Same as Fig. 5 except that latent heating profiles from the CSH look-up table (LUT) representing the corresponding geographic locations were used. See text for more details.

Fig. 7 Time (daily) series of latent heating profiles in K/day derived from the CSH heating algorithm for various geographic locations. The geographic areas are **(a)** the Central Pacific, **(b)** the East Pacific, **(c)** the South Pacific Convergence Zone, **(d)** the Indian Ocean, **(e)** the Atlantic Ocean, **(f)** South America, **(g)** Africa, **(h)** Australia, and **(i)** the TOGA COARE IFA region. Please note that the contour intervals are not always the same for Figs. 7(a) - 7(i).

Fig. 8 Monthly (February, 1998) mean latent heating profiles derived from the CSH heating algorithm for various geographic locations. Both approaches for selecting heating profiles from the look-up table (general land/ocean - like Fig. 5 or more detailed - like Fig. 6) are shown. The geographic areas are **(a)** the Central Pacific, **(b)** the East Pacific, **(c)** the South Pacific Convergence Zone, **(d)** the Indian Ocean, **(e)** the Atlantic Ocean (also shown using GCE GATE simulation profiles only), **(f)** South America, **(g)** Africa, **(h)** Australia, and **(i)** the TOGA COARE IFA region, Please note that the abscissa scales for Figs. 8(a) - 8(i) are not always the same.

Fig. 9 Same as Fig. 5 except using the Profile Heating Algorithm (Olson *et al.* 1999).

Fig. 10 Same as Fig. 5 except using the HH Algorithm (Yang and Smith, 1999a and b).

Fig. 11 Same as Fig. 8 except for variety of retrieval methods (Profile Heating algorithm, HH algorithm, CSH using the PR rainfall product, and CSH using the TMI rainfall product).

TABLES

Table 1 Summary of previous latent heating retrieval algorithms and their applications.

Table 2 The TMI and PR algorithm derived rainfall and stratiform percentage for the various geographic locations identified in Fig. 2. Entries are [TMI/PR] for rainfall and stratiform percentage.

Table 3 Major characteristics of latent heating profiles/structures estimated from three different heating retrieval algorithms and previous diagnostic budget studies.

Table 1

	Input	Cases	Resolution
Tao *et al.* (1991)	Surface Rainfall, Hydrometeor Profiles (cloud water, rain, cloud ice, snow and graupel) and Terminal velocity of rain, snow and graupel	GATE (1974), PRESTORM (1985)	200 - 300 km daily
Tao *et al.* (1993a)	Surface Rainfall and its stratiform percentage	GATE (1974), PRESTORM (1985), Typhoon Thelma (1987)	200 - 300 km daily
Olson *et al.* (1999)	Cloud modeled latent heating profiles and hydrometeor profiles	Hurricane Andrew (1992), TOGA COARE (1992-93)	25 - 50 km Instantaneously
Yang and Smith (1999a, b)	Hydrometeor Profiles (cloud water, rain, ice particles) and Cloud Vertical Velocities/ Terminal Velocity of rain and ice particles	TOGA COARE (1992-93) Global Tropical region (1992)	15 - 50 km Instantaneously 2.5^{o} x 2.5^{o} Monthly
Tao *et al.* (1999)	Surface Rainfall and its stratiform percentage	TOGA COARE (1992-93)	500 x 500 km weekly

Summary of previous latent heating algorithms and their applications

Table 2

	AVG Rainfall (mm/day)	Mean Stratiform (%)
TOGA COARE IFA Region	4.72/3.44	45/50
Central Pacific	11.64/7.07	54/61
East Pacific	7.75/4.16	52/58
South Pacific Convergence Zone	2.58/1.84	57/59
Indian Ocean	4.27/3.26	51/50
Atlantic Ocean	1.13/1.12	39/31
South America	4.79/4.14	25/44
Africa	1.85/1.59	24/32
Australia	2.20/1.92	30/49

GPROF and **PR** algorithm retrieved rainfall statistics - February 1998

Table 3

	CSH Algorithm	GPROF Heating Algorithm	HH Algorithm	Budget Studies
Magnitude (Maximum Heating rates)	4-6* K day^{-1} per 1 cm day^{-1}	4-6 K day^{-1} per 1 cm day^{-1}	4-6 K day^{-1} per 1 cm day^{-1}	4-10 K day^{-1} per 1 cm day^{-1}
Horizontal Variation	Similar patterns as surface rainfall (i.e. ITCZ over Pacific and an SPCZ). Relative strong low-level cooling over portion of Pacific Ocean	Similar patterns as surface rainfall (i.e. ITCZ over Pacific and an SPCZ). Strong low-middle cooling from 25-35 N in Pacific and Atlantic Oceans	Similar patterns as surface rainfall (i.e. ITCZ over Pacific and an SPCZ). Area with weak low-level heating and cooling quite large	Inadequate observations
Maximum Heating Level	Single maximum in all geographic locations. Higher (8 km level) in Pacific and Indian, and SPCZ. Lower in Africa, Australia and S. America	Multiple peaks over most geographic locations except Africa. Its higher maximum is lower than the CSH estimated over Pacific, Indian Ocean and TOGA COARE	Multiple peaks over most geographic locations except SPCZ and Pacific Ocean. Its higher maximum is almost the same as the CSH estimated	Single Maximum in GATE, AMEX, TOGA COARE, ABLE, PRESTORM and others. Higher in TOGA COARE. Lower in AMEX and GATE, ABLE.
Notes	No temporal variation. No cooling between active convective events. No temporal variation in low levels (i.e. diurnal variation)	Maximum heating level does not vary over various geographic locations. Strong cooling in mid-level over subtropics	No relative strong low-level heating over land and cooling over Oceans	Need more observations over various geographic locations in different seasons

* 4-8 K day^{-1} per 1 cm day^{-1} if different heating profiles are selected from look-up table.

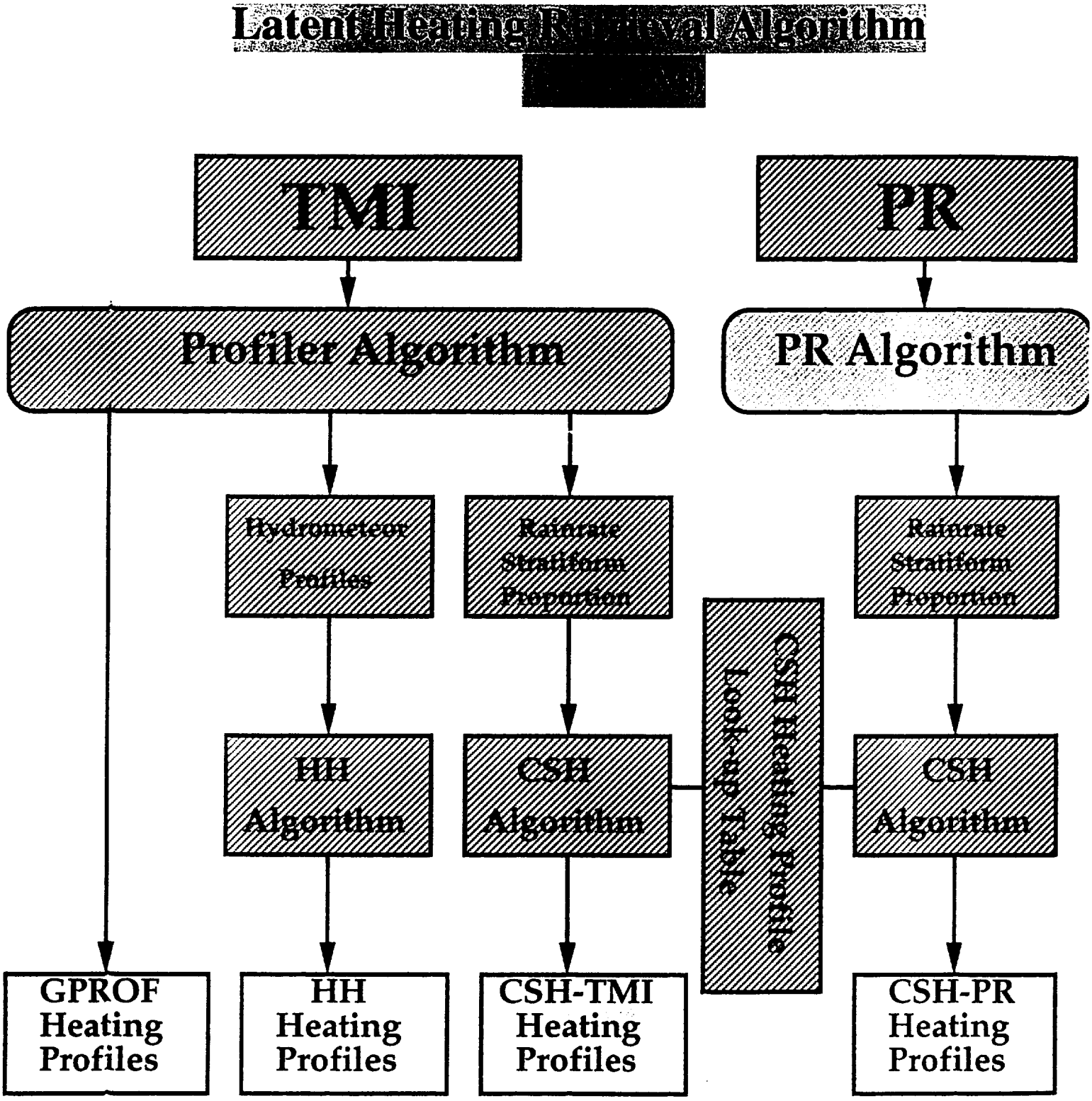
Latent Heating R val Algorithm
TMI
PR
Profiler Algorithm
PR Algorithm
Hydrometeor Profiles
Rainrate Stratiform Proportion
Rainrate Stratiform Proportion
HH Algorithm
CSH Algorithm
CSH Algorithm
Look-up Table
CSH Heating Profile
GPROF Heating Profiles
HH Heating Profiles
CSH-TMI Heating Profiles
CSH-PR Heating Profiles

Fig. 1

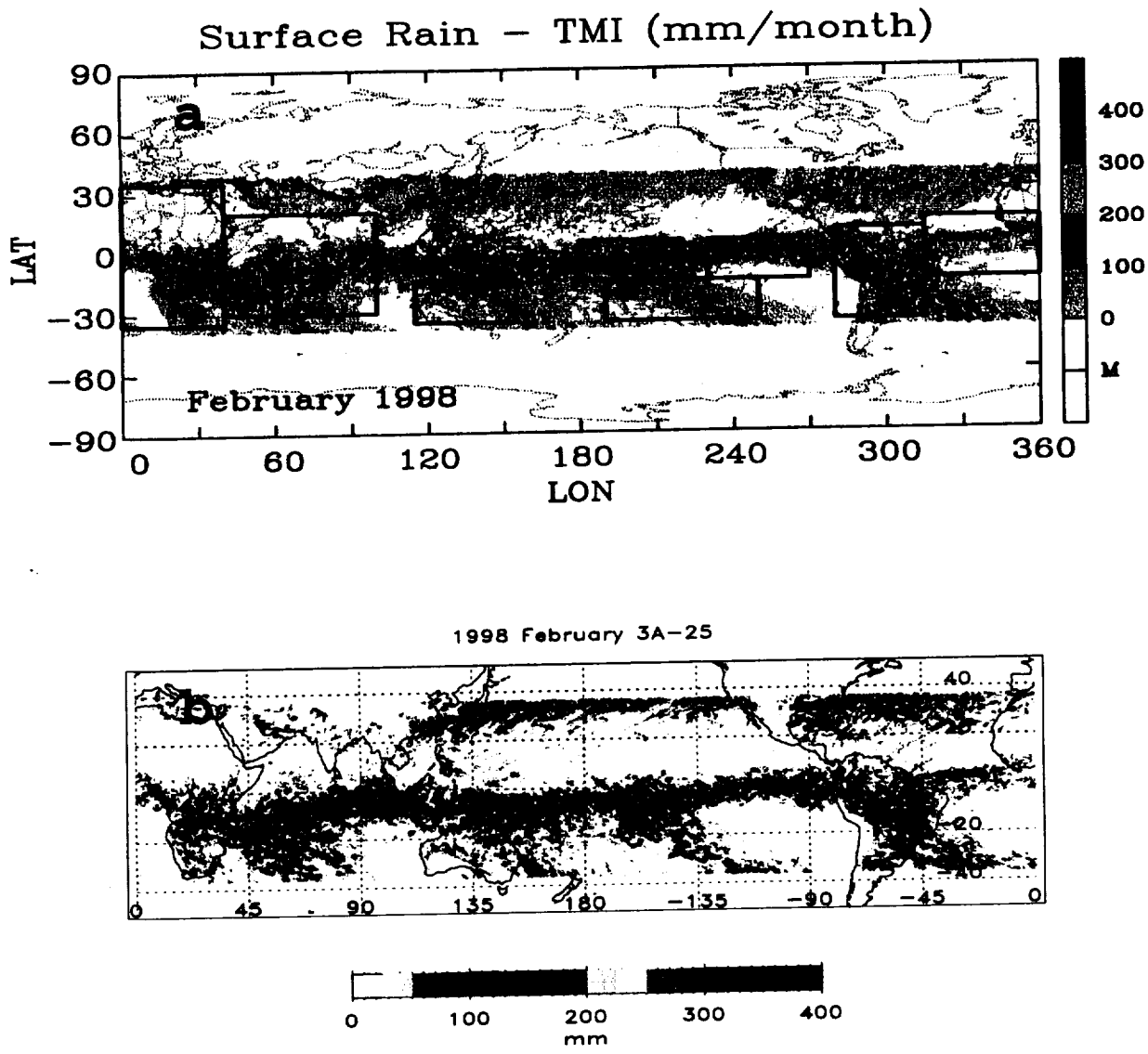
Surface Rain – TMI (mm/month)
a
February 1998
LAT
LON
90
60
30
0
−30
−60
−90
0
60
120
180
240
300
360
400
300
200
100
0
M
1998 February 3A-25
b
40
20
0
45
90
135
180
−135
−90
−45
0
0
100
200
300
400
mm

Fig. 2

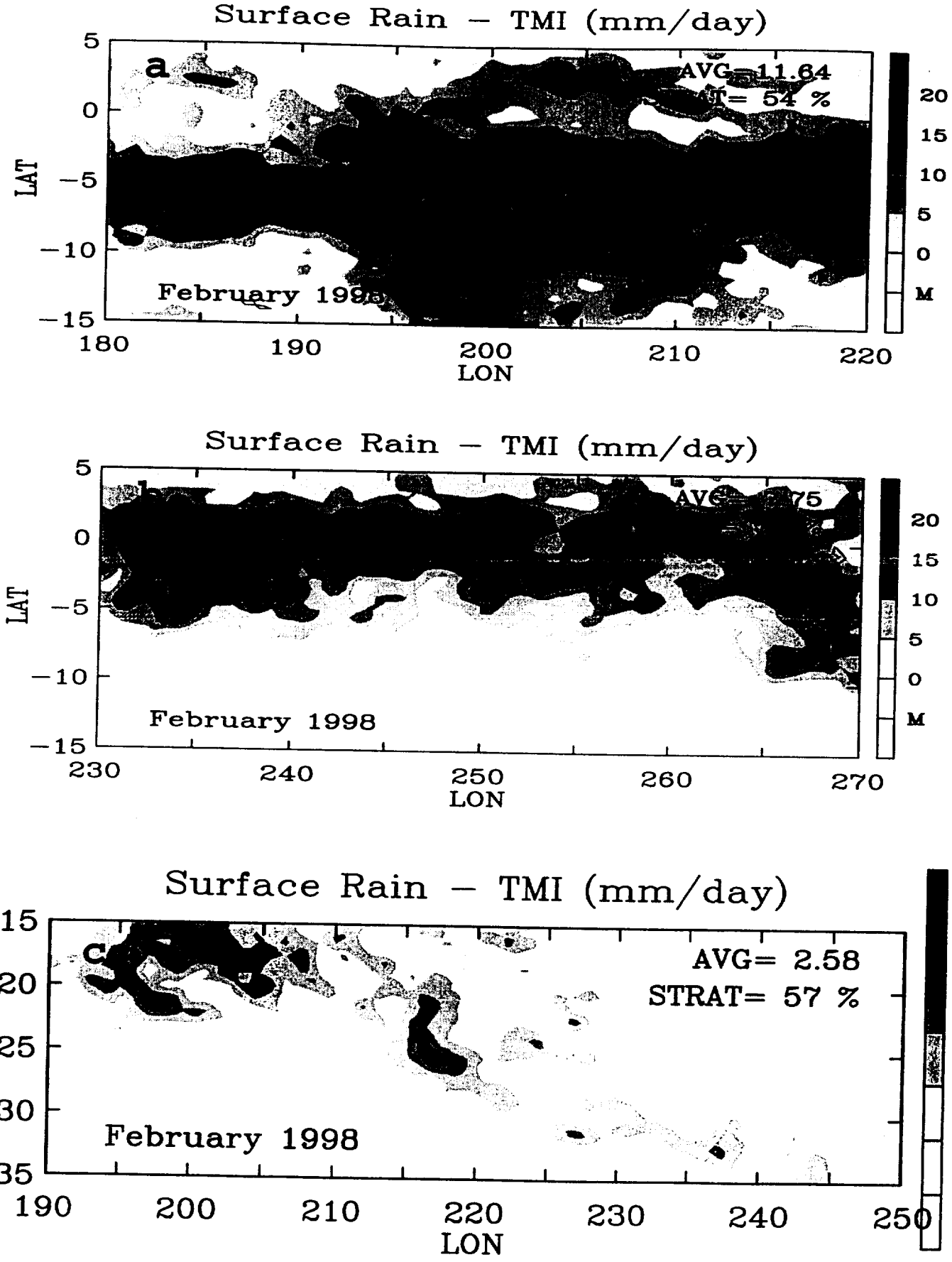
Surface Rain – TMI (mm/day)
a
AVG= 11.64
STRAT= 54 %
February 1998
LAT
LON
5
0
−5
−10
−15
180
190
200
210
220
20
15
10
5
0
M
Surface Rain – TMI (mm/day)
February 1998
LAT
LON
230
240
250
260
270
Surface Rain – TMI (mm/day)
c
AVG= 2.58
STRAT= 57 %
February 1998
LAT
LON
−15
−20
−25
−30
−35
190
200
210
220
230
240
250

Fig. 3

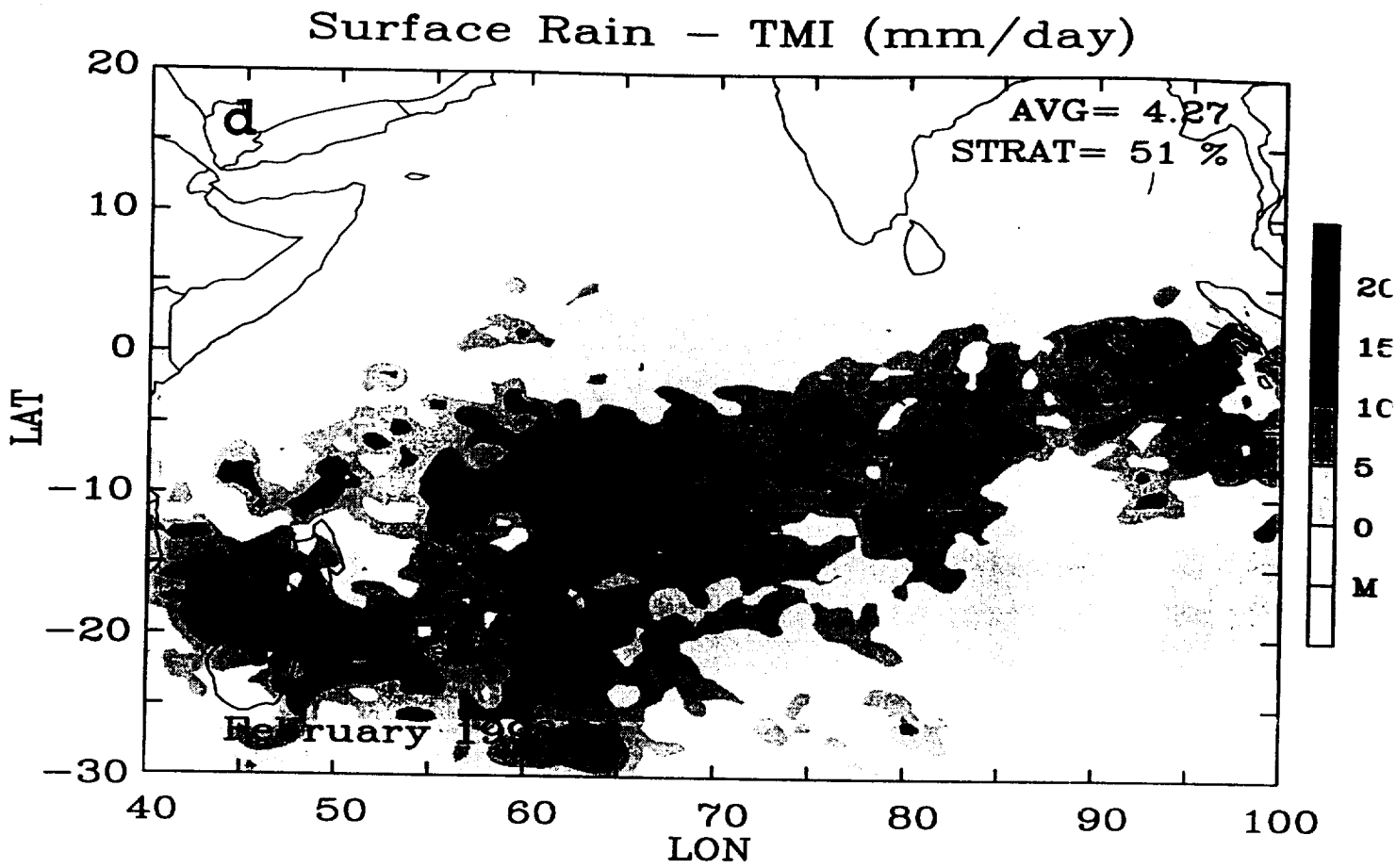
Surface Rain – TMI (mm/day)
d
AVG= 4.27
STRAT= 51 %
20
10
0
−10
−20
−30
LAT
40
50
60
70
80
90
100
LON
20
15
10
5
0
M

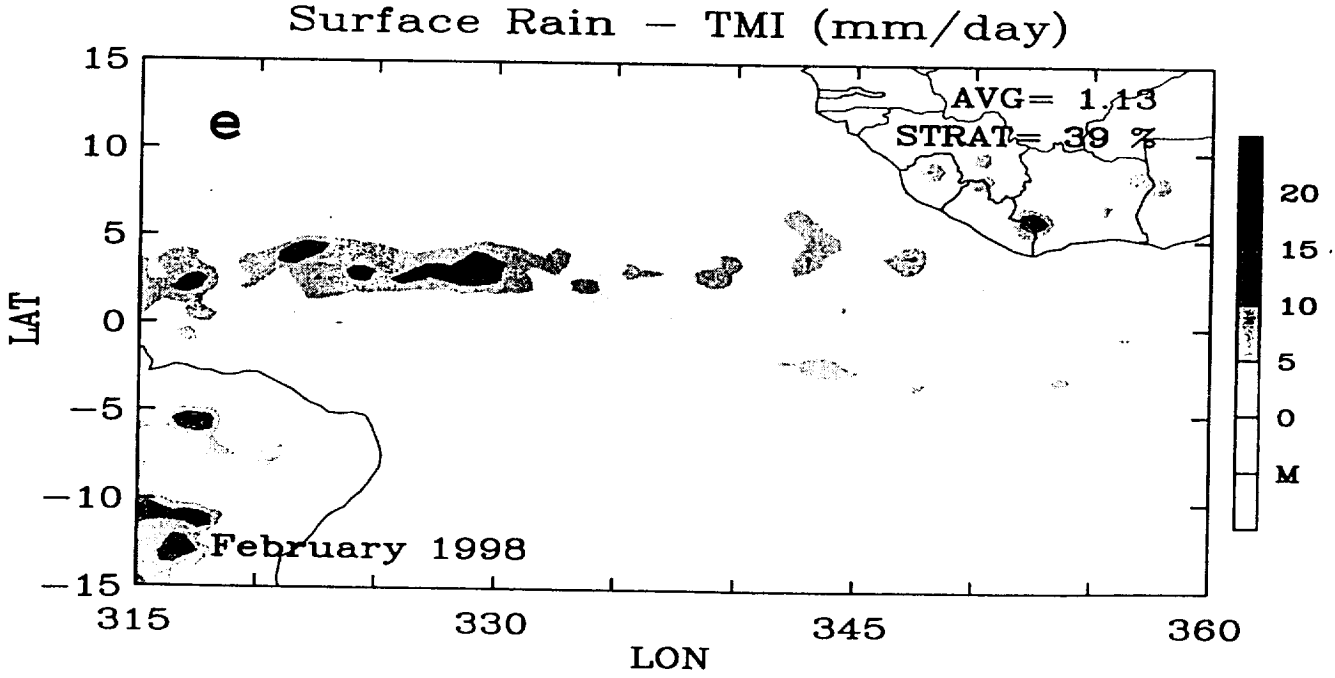
Surface Rain – TMI (mm/day)
e
AVG= 1.13
STRAT= 39 %
15
10
5
0
−5
−10
−15
LAT
315
330
345
360
LON
February 1998
20
15
10
5
0
M

Fig. 3 (Cont)

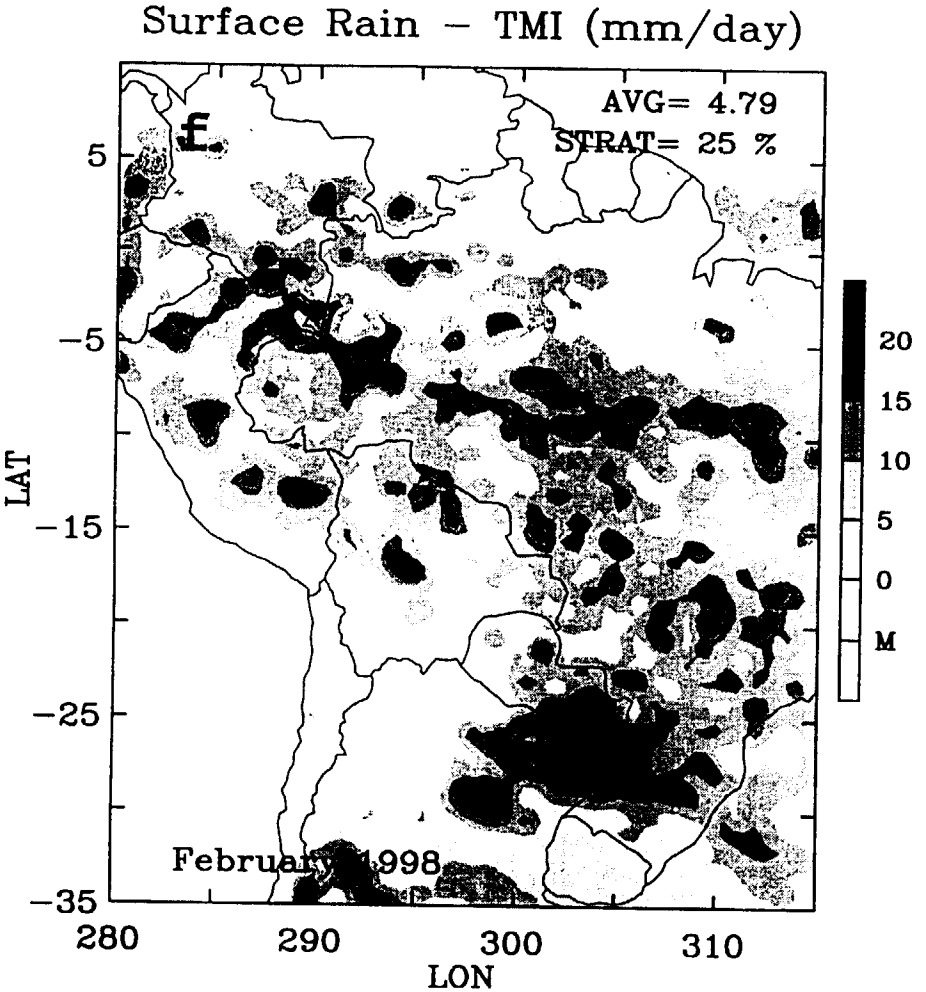
Surface Rain – TMI (mm/day)
f.
AVG= 4.79
STRAT= 25 %
February 1998
LAT
LON
5
-5
-15
-25
-35
280
290
300
310
20
15
10
5
0
M

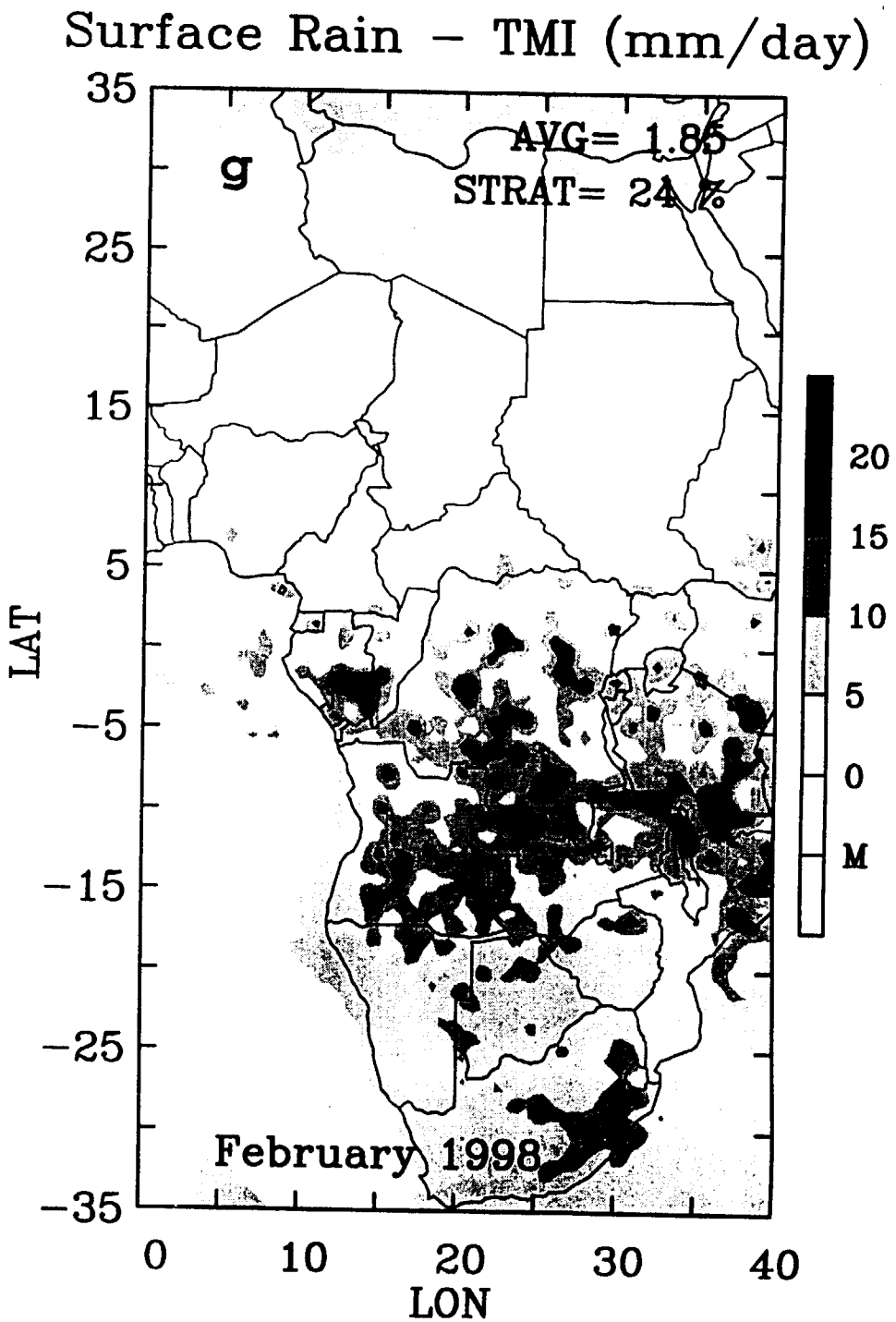
Surface Rain – TMI (mm/day)
g
AVG= 1.85
STRAT= 24 %
February 1998
LAT
LON
35
25
15
5
-5
-15
-25
-35
0
10
20
30
40
20
15
10
5
0
M

Fig. 3 (Cont)

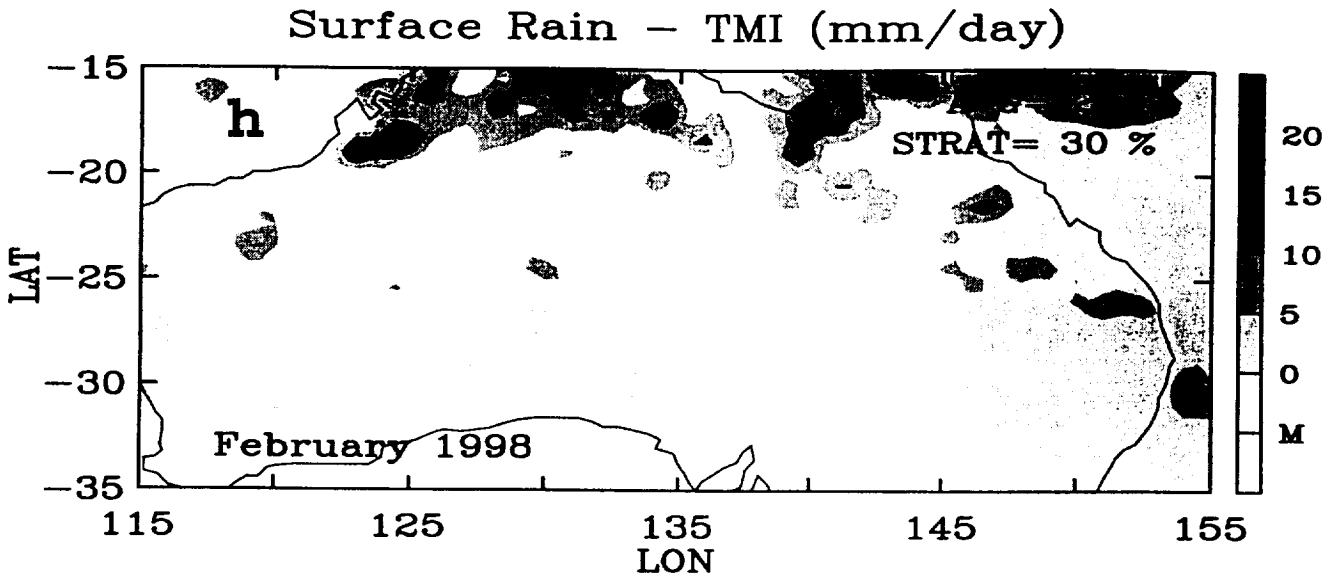
Surface Rain – TMI (mm/day)
h
STRAT= 30 %
February 1998
LAT
LON
−15
−20
−25
−30
−35
115
125
135
145
155
20
15
10
5
0
M

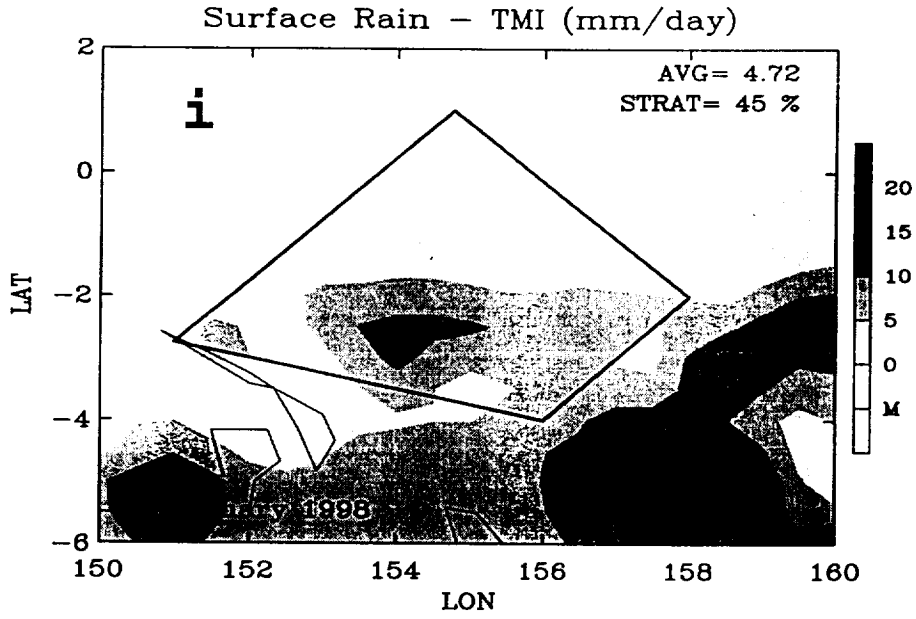
Surface Rain – TMI (mm/day)
i
AVG= 4.72
STRAT= 45 %
LAT
LON
2
0
−2
−4
−6
150
152
154
156
158
160
20
15
10
5
0
M

Fig. 3 (Cont)

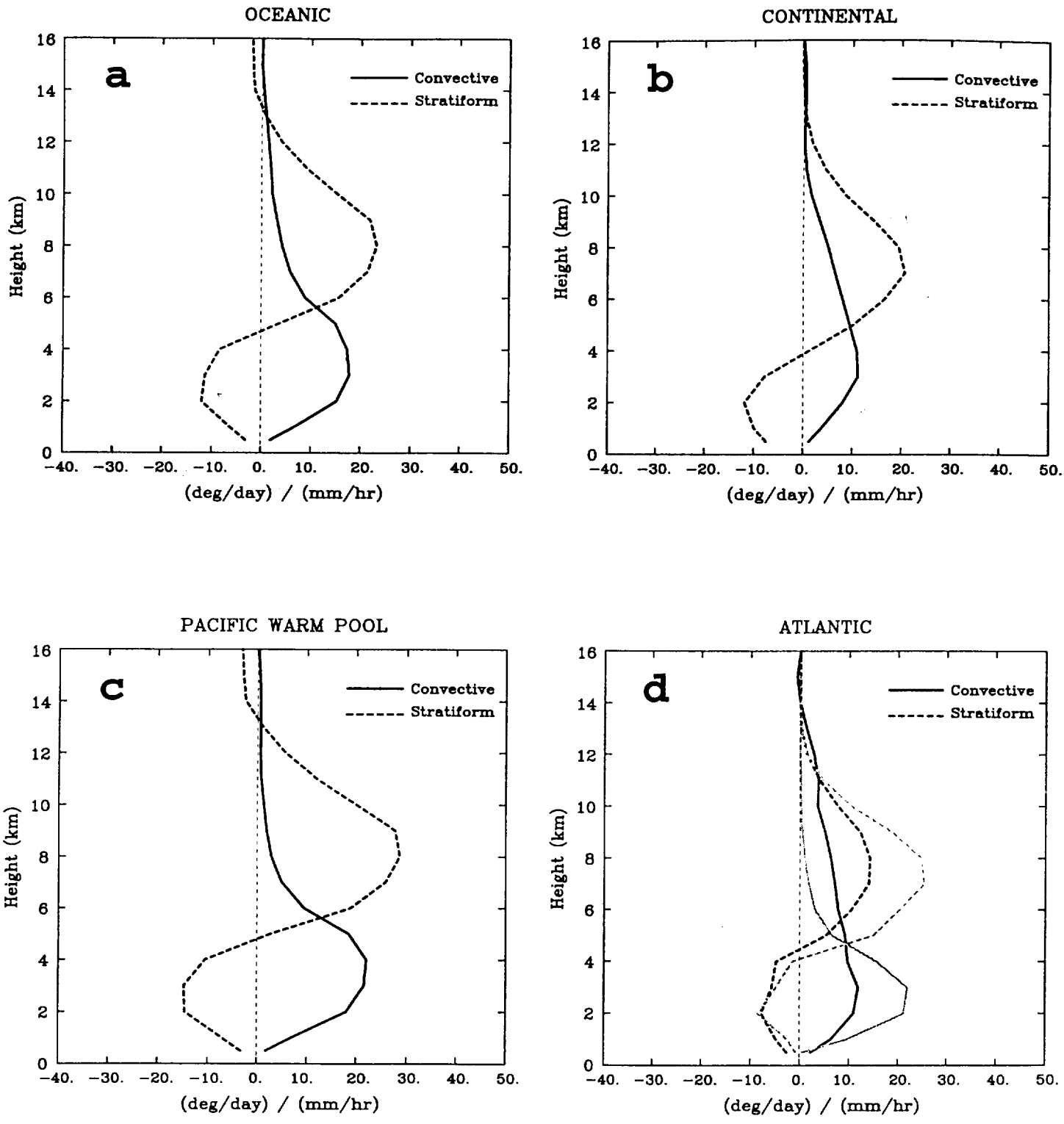
OCEANIC
a
Convective
Stratiform
Height (km)
(deg/day) / (mm/hr)
CONTINENTAL
b
Convective
Stratiform
Height (km)
(deg/day) / (mm/hr)
PACIFIC WARM POOL
c
Convective
Stratiform
Height (km)
(deg/day) / (mm/hr)
ATLANTIC
d
Convective
Stratiform
Height (km)
(deg/day) / (mm/hr)

Fig. 4

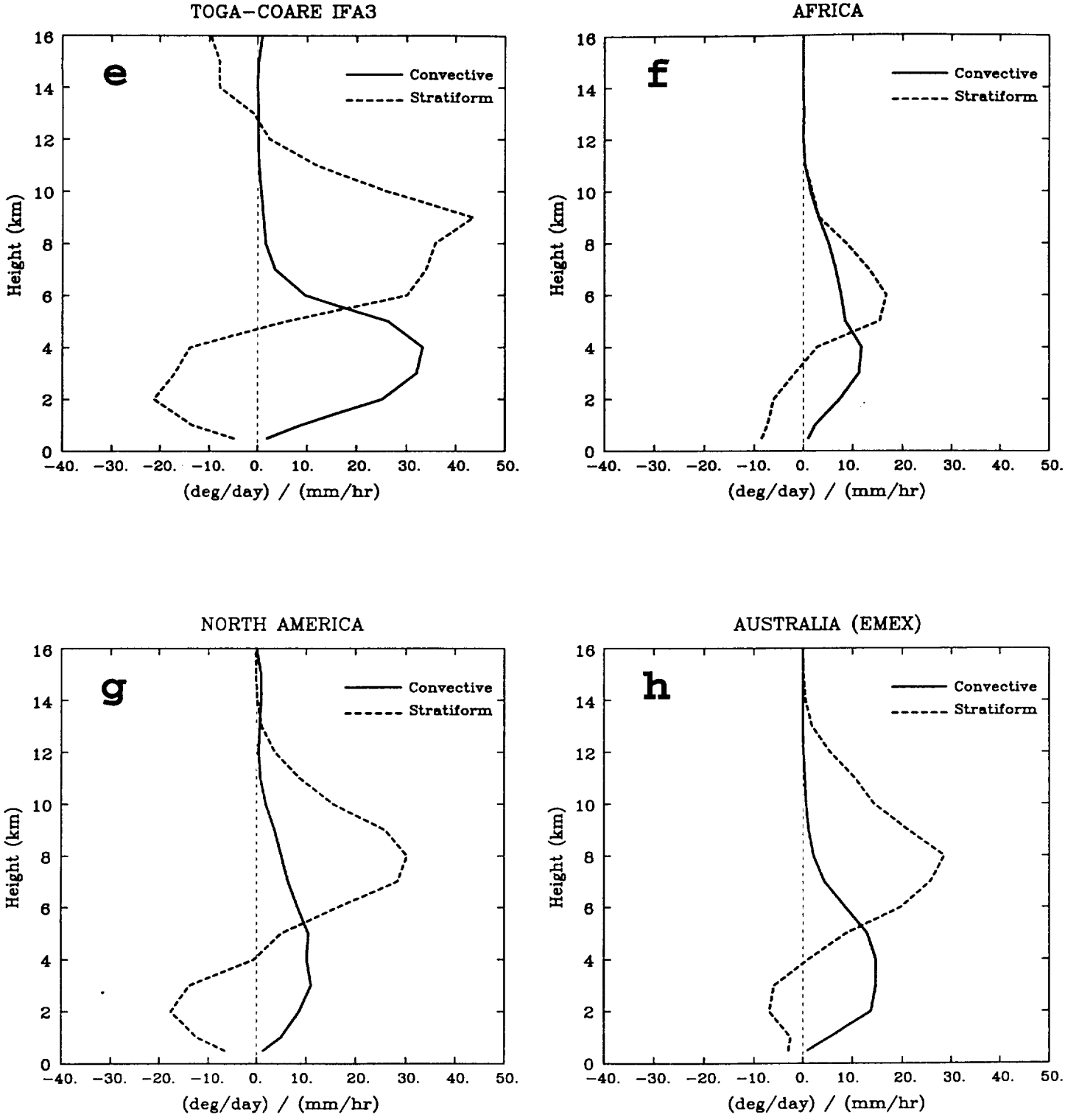
TOGA–COARE IFA3
e
Convective
Stratiform
Height (km)
(deg/day) / (mm/hr)
AFRICA
f
Convective
Stratiform
Height (km)
(deg/day) / (mm/hr)
NORTH AMERICA
g
Convective
Stratiform
Height (km)
(deg/day) / (mm/hr)
AUSTRALIA (EMEX)
h
Convective
Stratiform
Height (km)
(deg/day) / (mm/hr)

Fig. 4 (Cont)

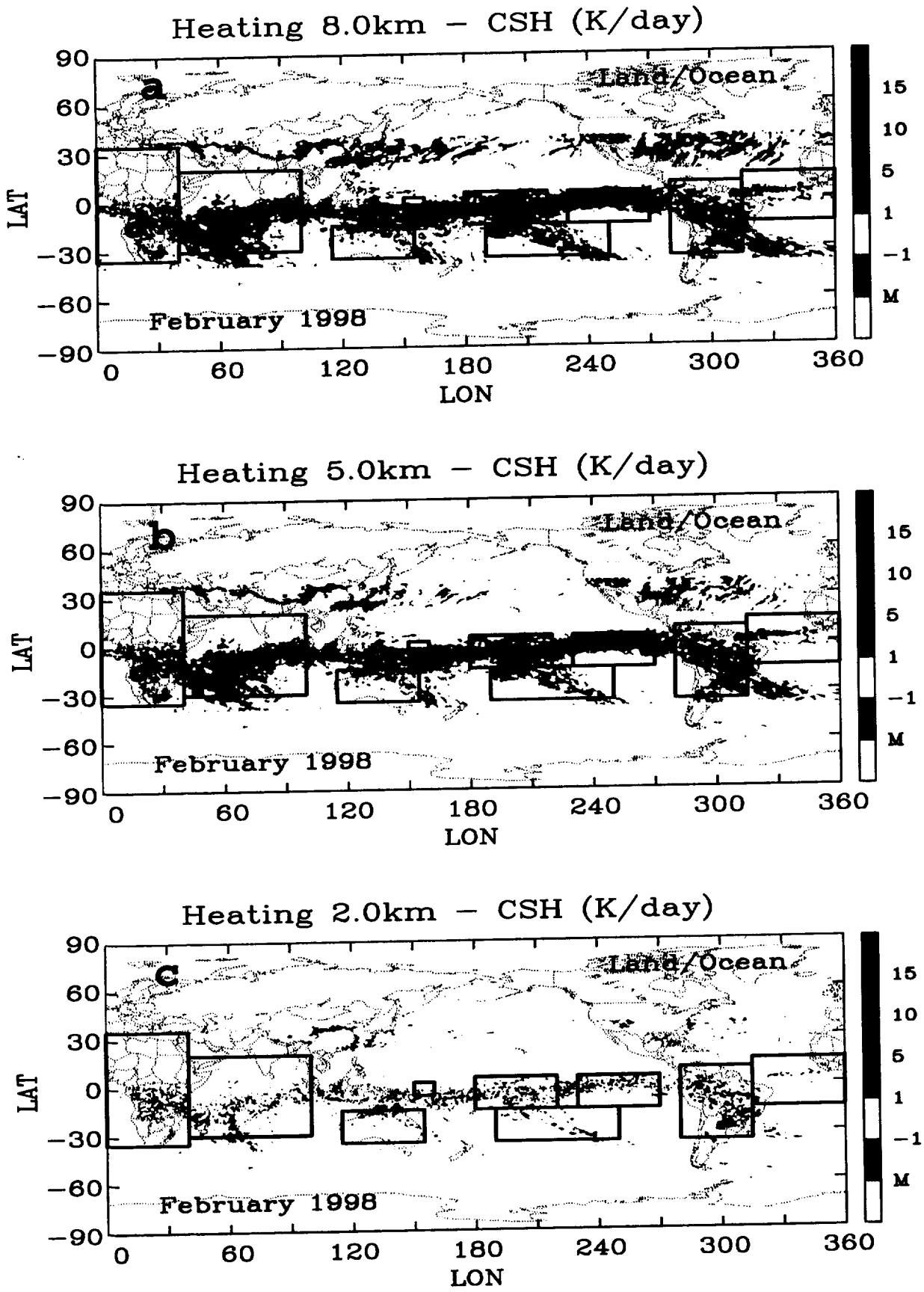
Heating 8.0km – CSH (K/day)
a
Land/Ocean
February 1998
LAT
LON
90
60
30
0
−30
−60
−90
0
60
120
180
240
300
360
15
10
5
1
−1
M
Heating 5.0km – CSH (K/day)
b
Land/Ocean
February 1998
LAT
LON
Heating 2.0km – CSH (K/day)
c
Land/Ocean
February 1998
LAT
LON

Fig. 5

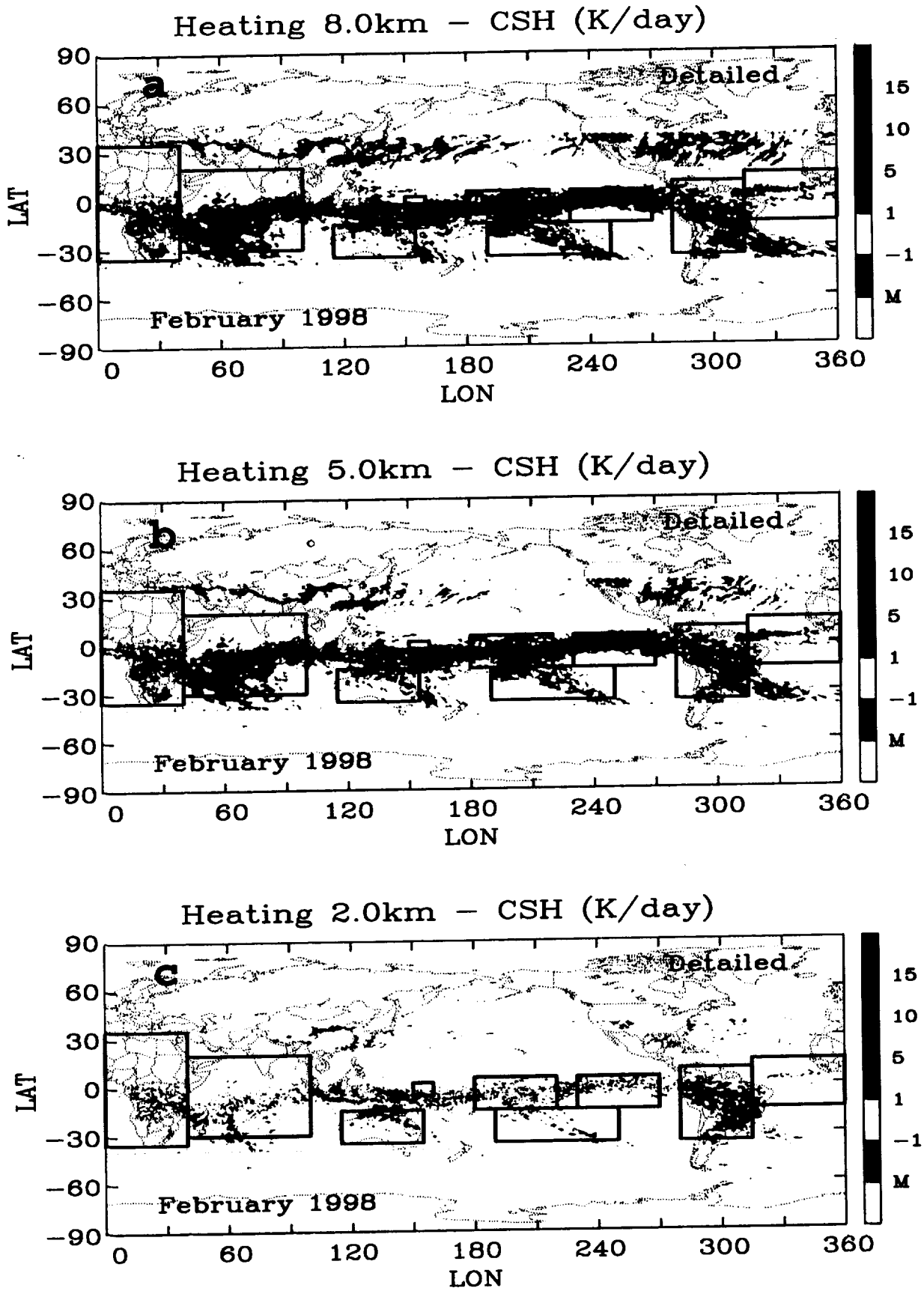
Heating 8.0km – CSH (K/day)
a
Detailed
February 1998
LAT
LON
90
60
30
0
−30
−60
−90
0
60
120
180
240
300
360
15
10
5
1
−1
M
Heating 5.0km – CSH (K/day)
b
Detailed
February 1998
LAT
LON
Heating 2.0km – CSH (K/day)
c
Detailed
February 1998
LAT
LON

Fig. 6

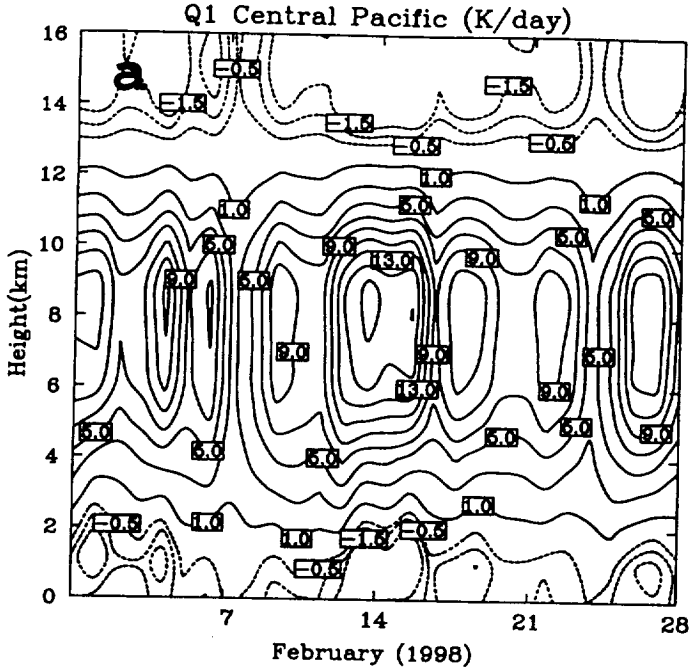
Q1 Central Pacific (K/day)
a
Height(km)
February (1998)

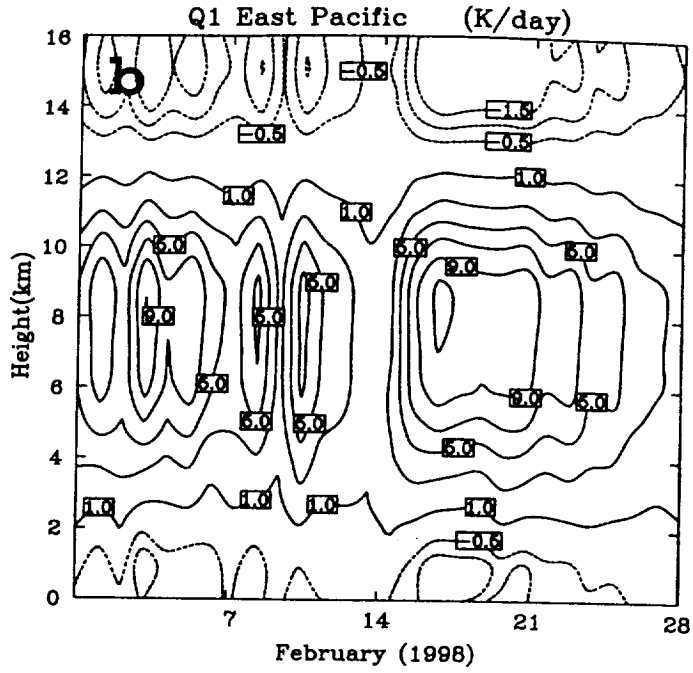
Q1 East Pacific (K/day)
b
Height(km)
February (1998)

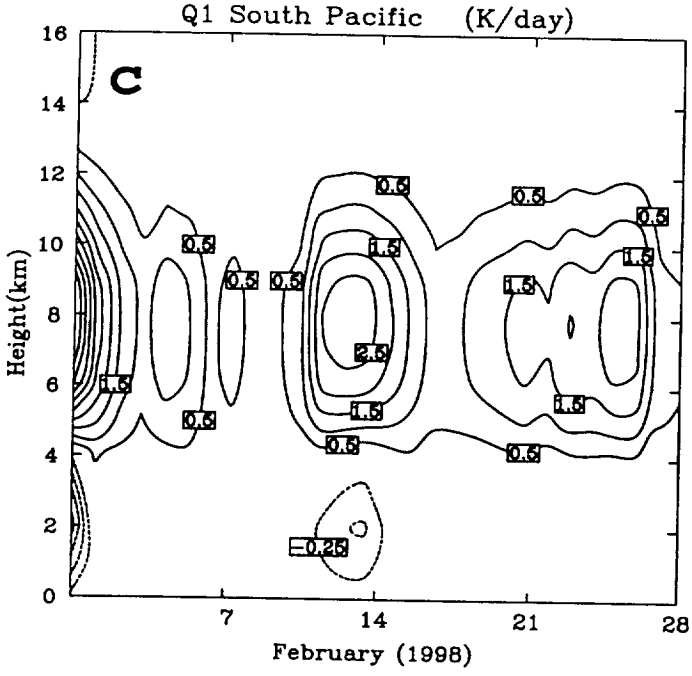
Q1 South Pacific (K/day)
c
Height(km)
February (1998)

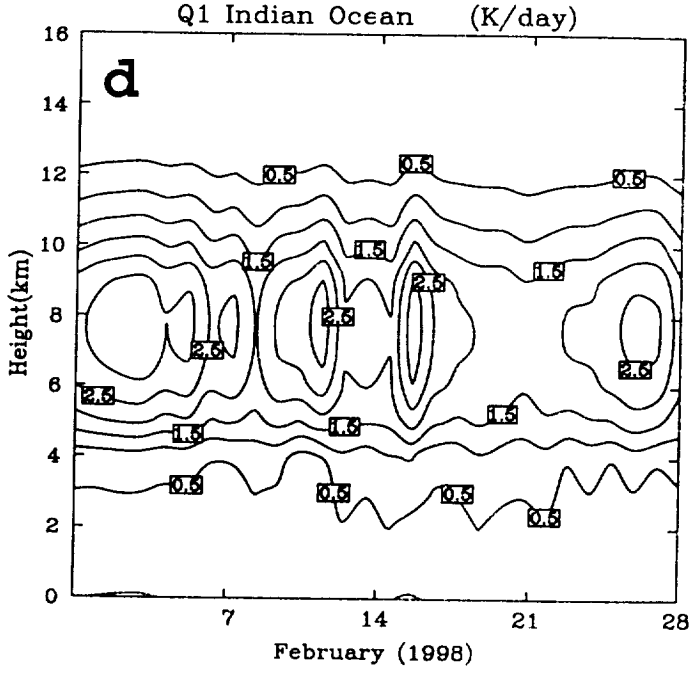
Q1 Indian Ocean (K/day)
d
Height(km)
February (1998)

Fig. 7

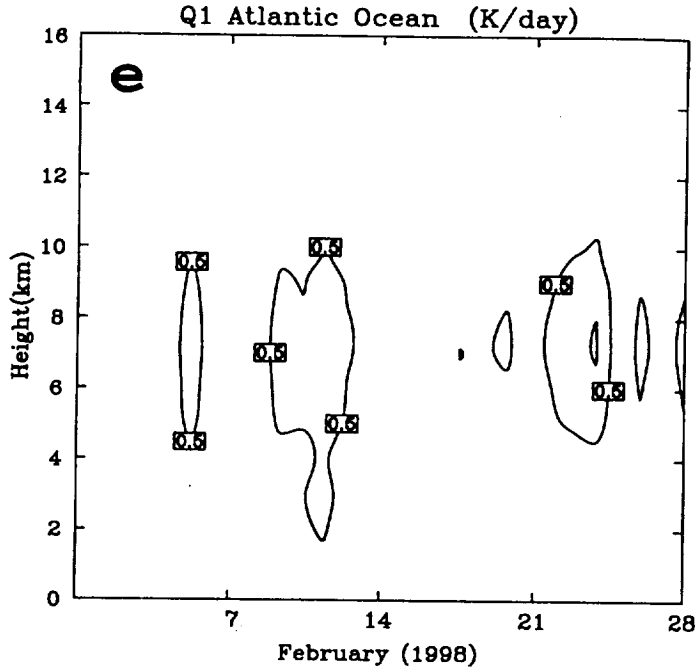
Q1 Atlantic Ocean (K/day)
e
Height(km)
February (1998)

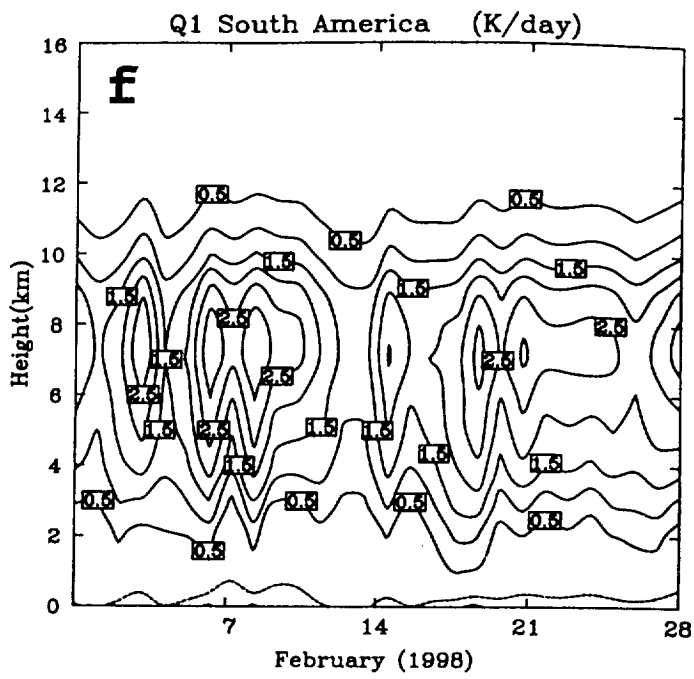
Q1 South America (K/day)
f
Height(km)
February (1998)

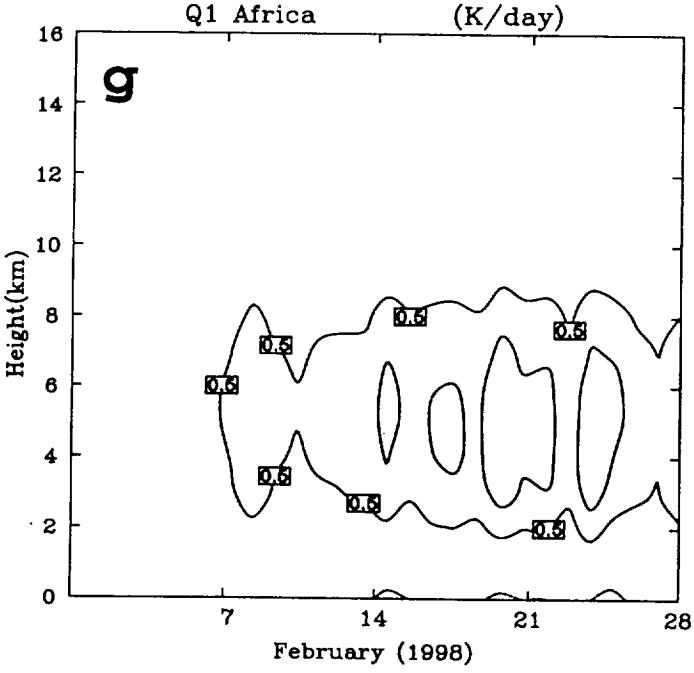
Q1 Africa (K/day)
g
Height(km)
February (1998)

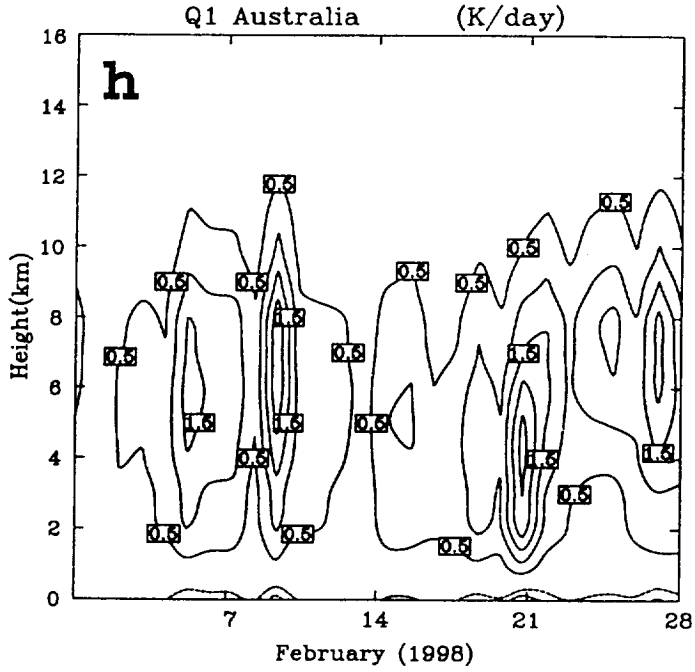
Q1 Australia (K/day)
h
Height(km)
February (1998)

Fig. 7 (Cont)

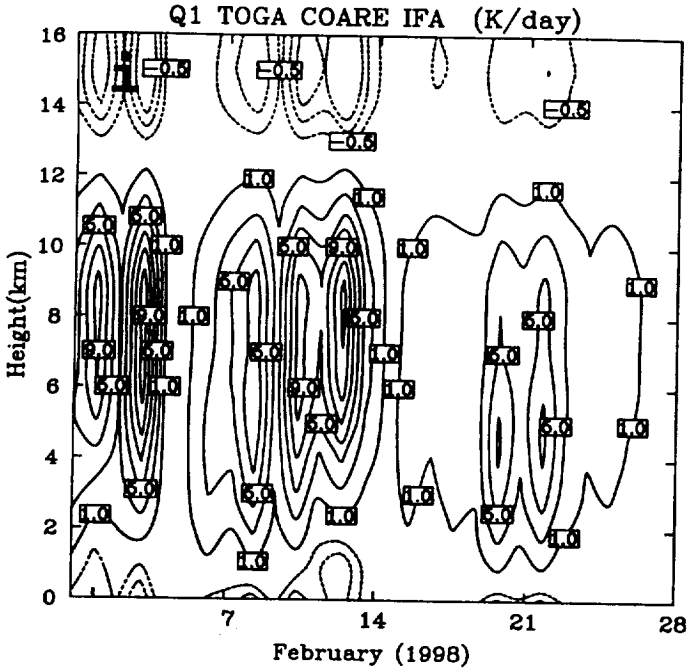
Q1 TOGA COARE IFA (K/day)
Height(km)
February (1998)
16
14
12
10
8
6
4
2
0
7
14
21
28

Fig. 7 (Cont)

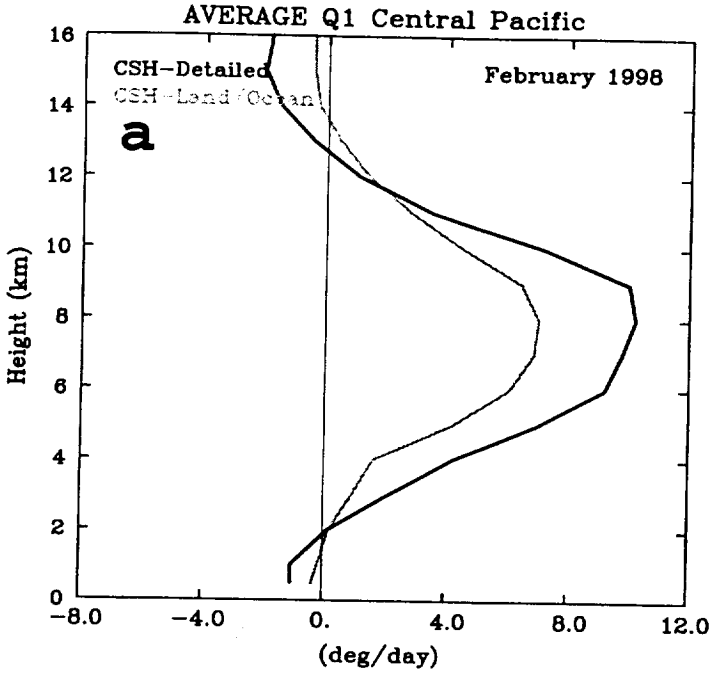
AVERAGE Q1 Central Pacific
CSH-Detailed
CSH-Land/Ocean
February 1998
a
Height (km)
(deg/day)

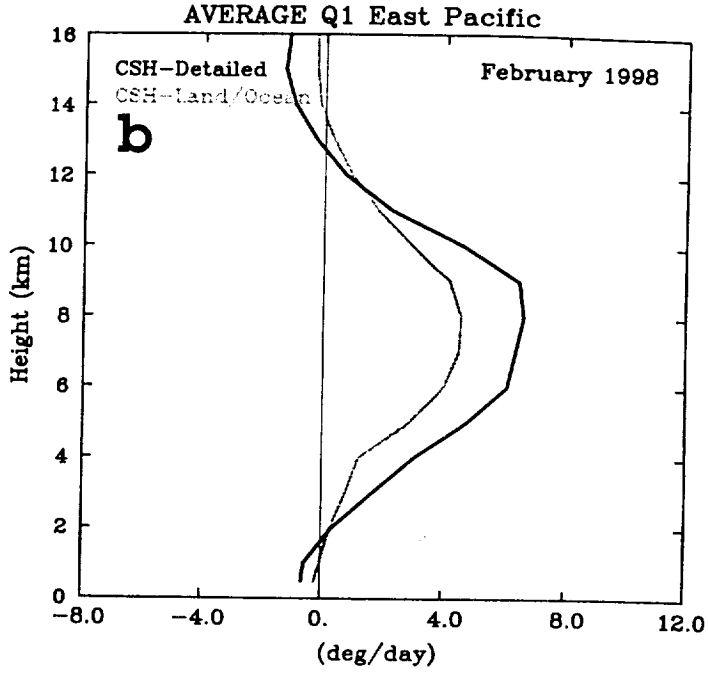
AVERAGE Q1 East Pacific
CSH-Detailed
CSH-Land/Ocean
February 1998
b
Height (km)
(deg/day)

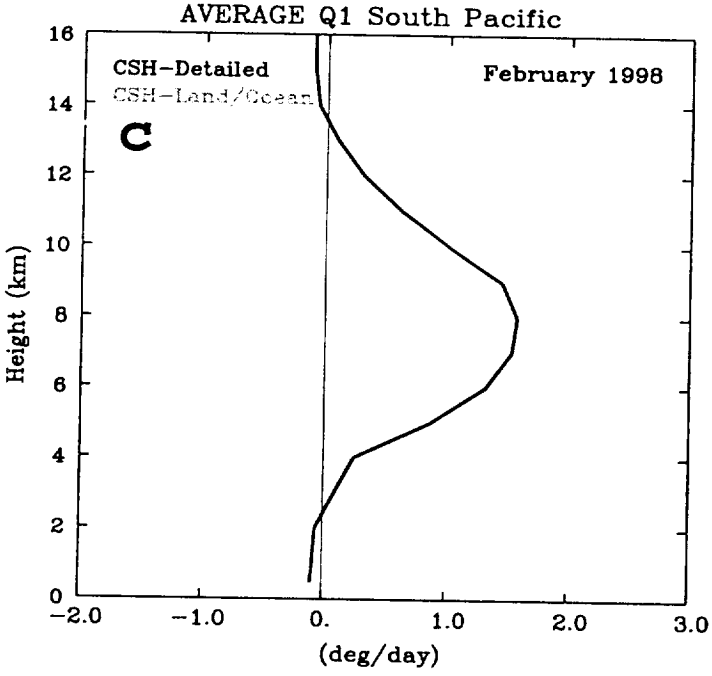
AVERAGE Q1 South Pacific
CSH-Detailed
CSH-Land/Ocean
February 1998
c
Height (km)
(deg/day)

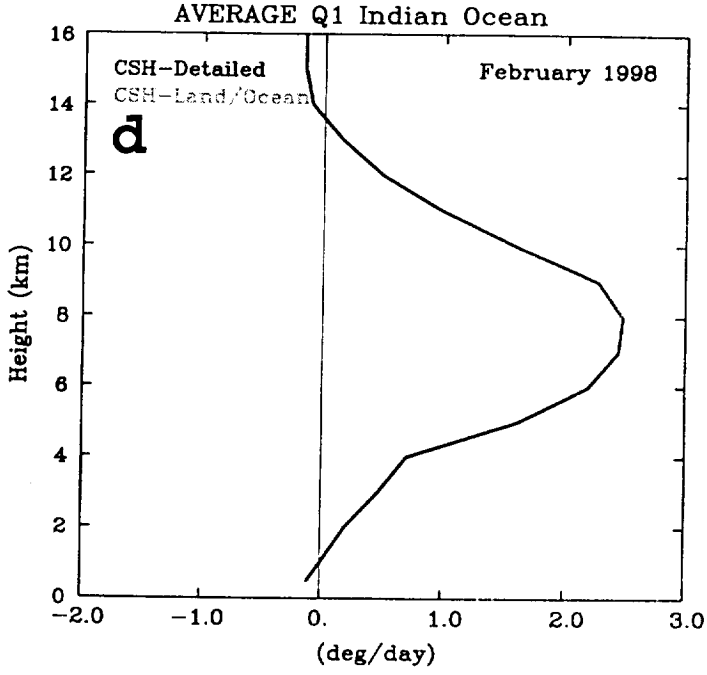
AVERAGE Q1 Indian Ocean
CSH-Detailed
CSH-Land/Ocean
February 1998
d
Height (km)
(deg/day)

Fig. 8

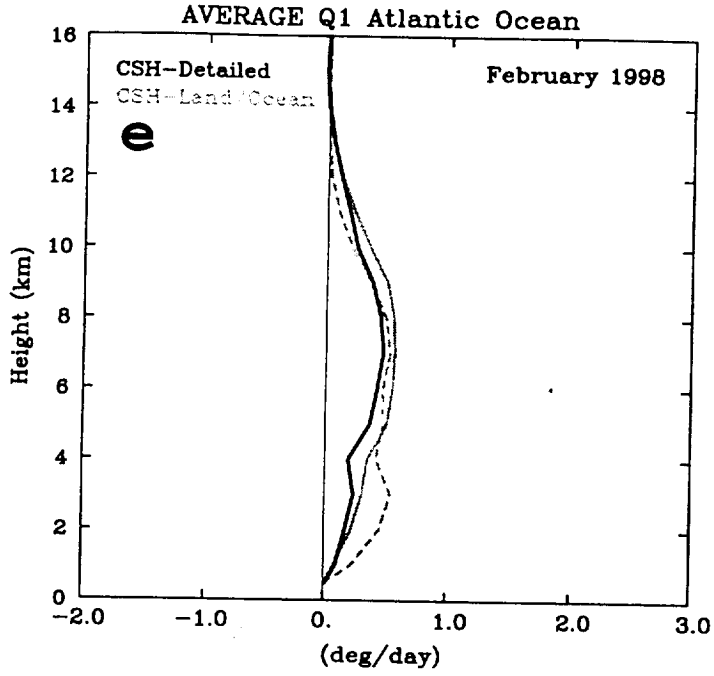
AVERAGE Q1 Atlantic Ocean
CSH-Detailed
CSH-Land/Ocean
February 1998
e
Height (km)
(deg/day)

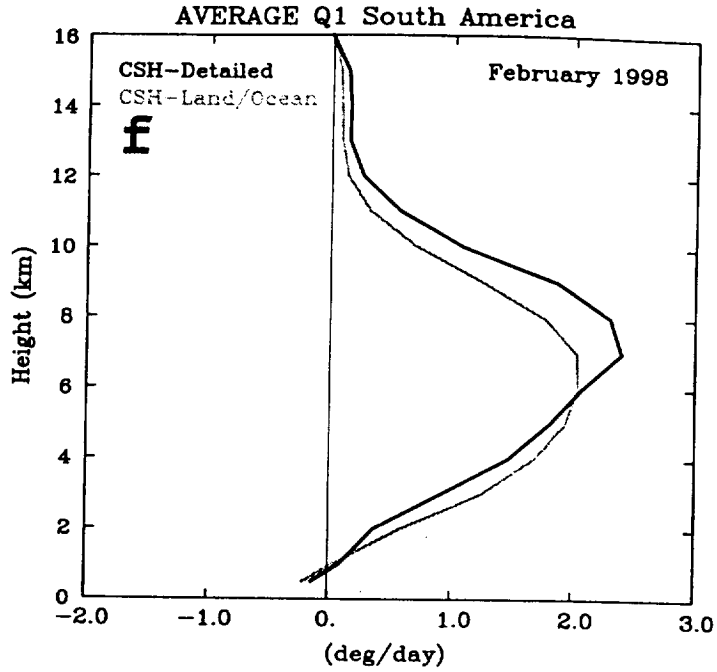
AVERAGE Q1 South America
CSH-Detailed
CSH-Land/Ocean
February 1998
f
Height (km)
(deg/day)

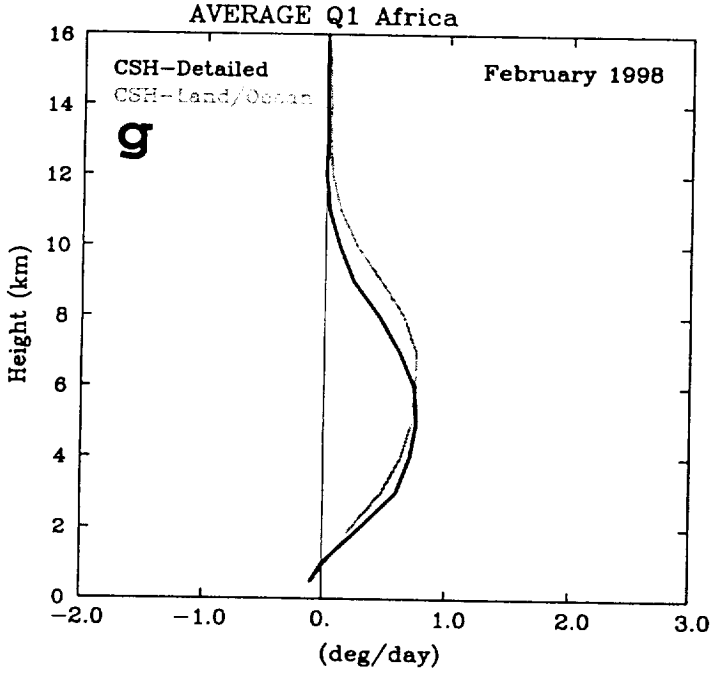
AVERAGE Q1 Africa
CSH-Detailed
CSH-Land/Ocean
February 1998
g
Height (km)
(deg/day)

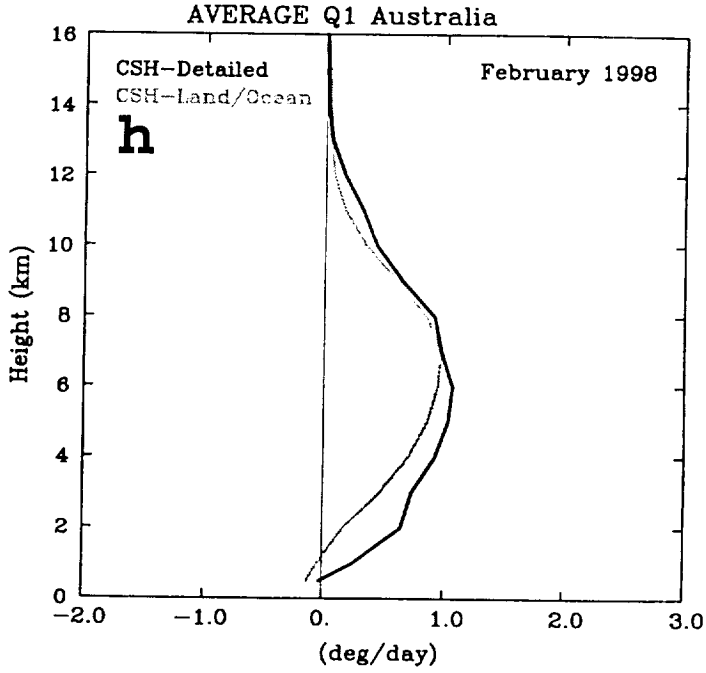
AVERAGE Q1 Australia
CSH-Detailed
CSH-Land/Ocean
February 1998
h
Height (km)
(deg/day)

Fig. 8 (Cont)

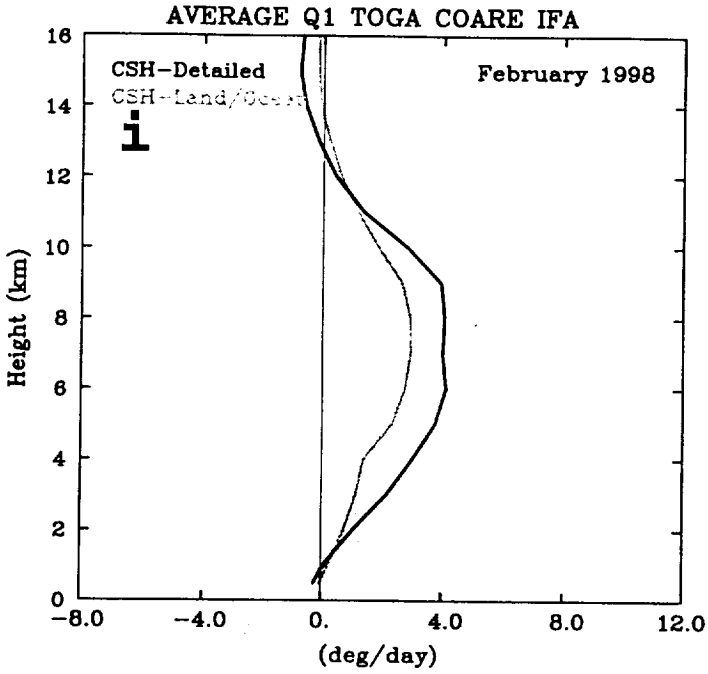
AVERAGE Q1 TOGA COARE IFA
CSH-Detailed
February 1998
Height (km)
16
14
12
10
8
6
4
2
0
−8.0
−4.0
0.
4.0
8.0
12.0
(deg/day)

Fig. 8 (Cont)

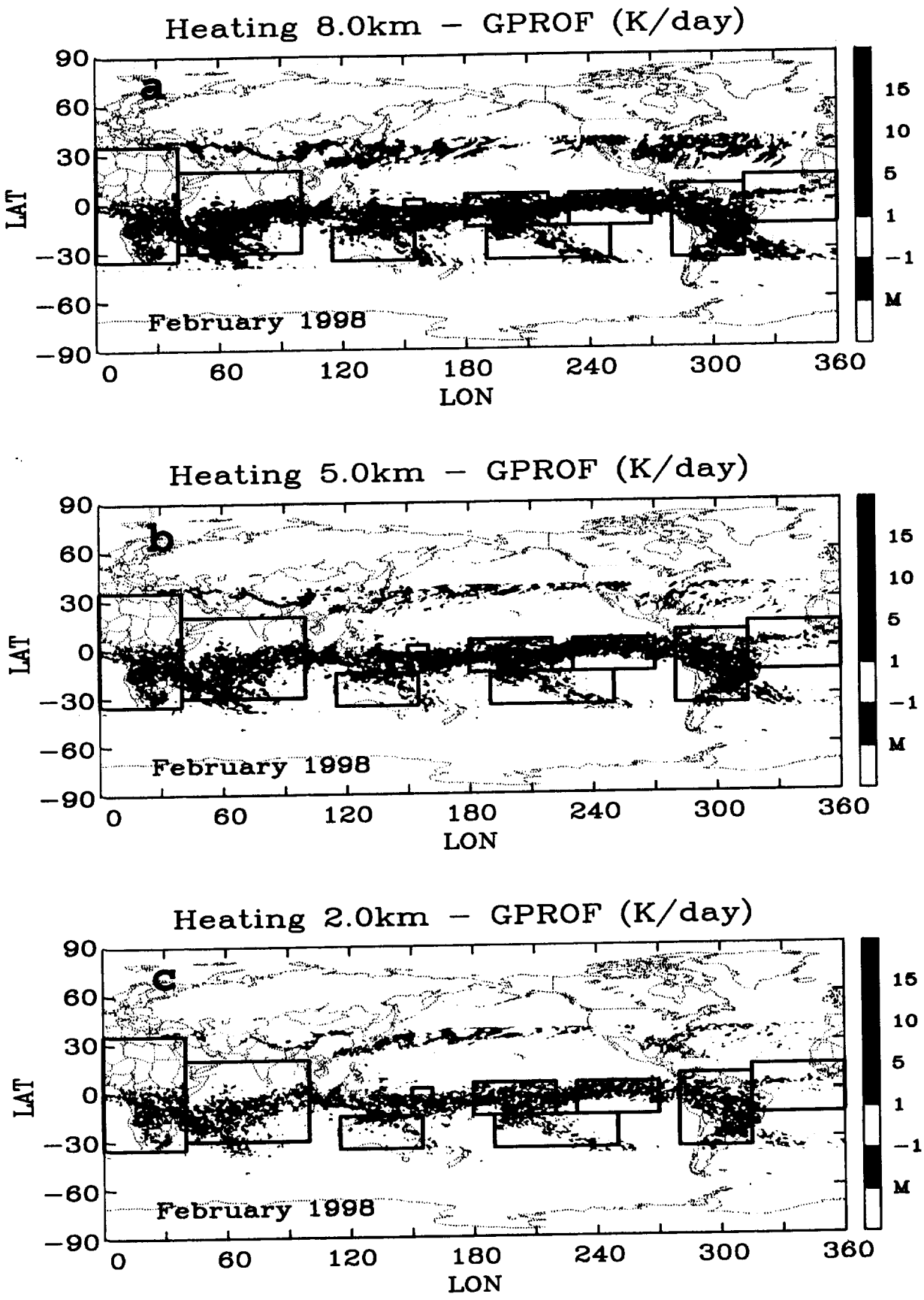
Heating 8.0km – GPROF (K/day)
a
February 1998
Heating 5.0km – GPROF (K/day)
b
February 1998
Heating 2.0km – GPROF (K/day)
c
February 1998
LAT
LON
90
60
30
0
−30
−60
−90
0
60
120
180
240
300
360
15
10
5
1
−1
M

Fig. 9

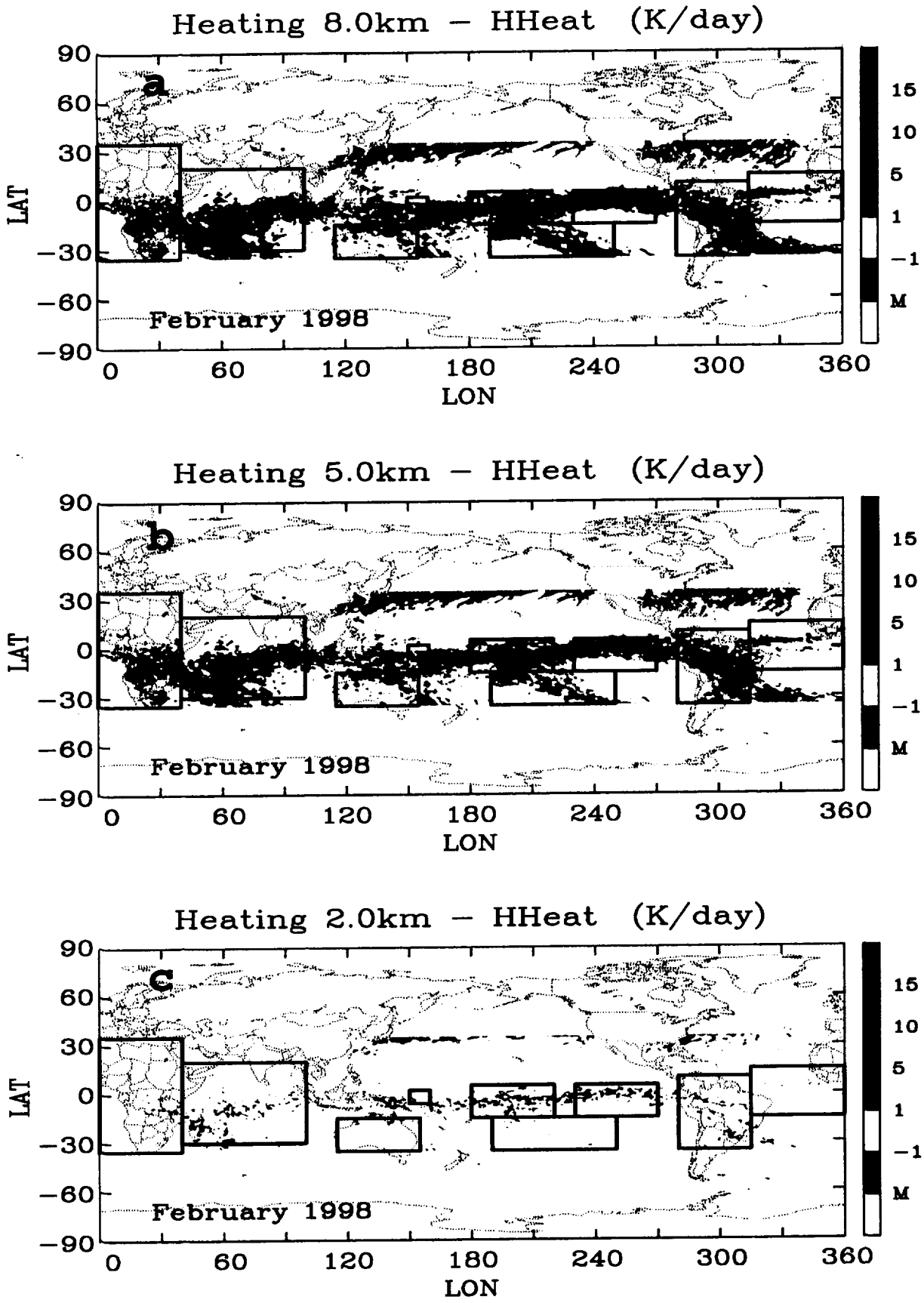
Heating 8.0km – HHeat (K/day)
a
February 1998
Heating 5.0km – HHeat (K/day)
b
February 1998
Heating 2.0km – HHeat (K/day)
c
February 1998
LAT
LON
90
60
30
0
−30
−60
−90
0
60
120
180
240
300
360
15
10
5
1
−1
M

Fig. 10

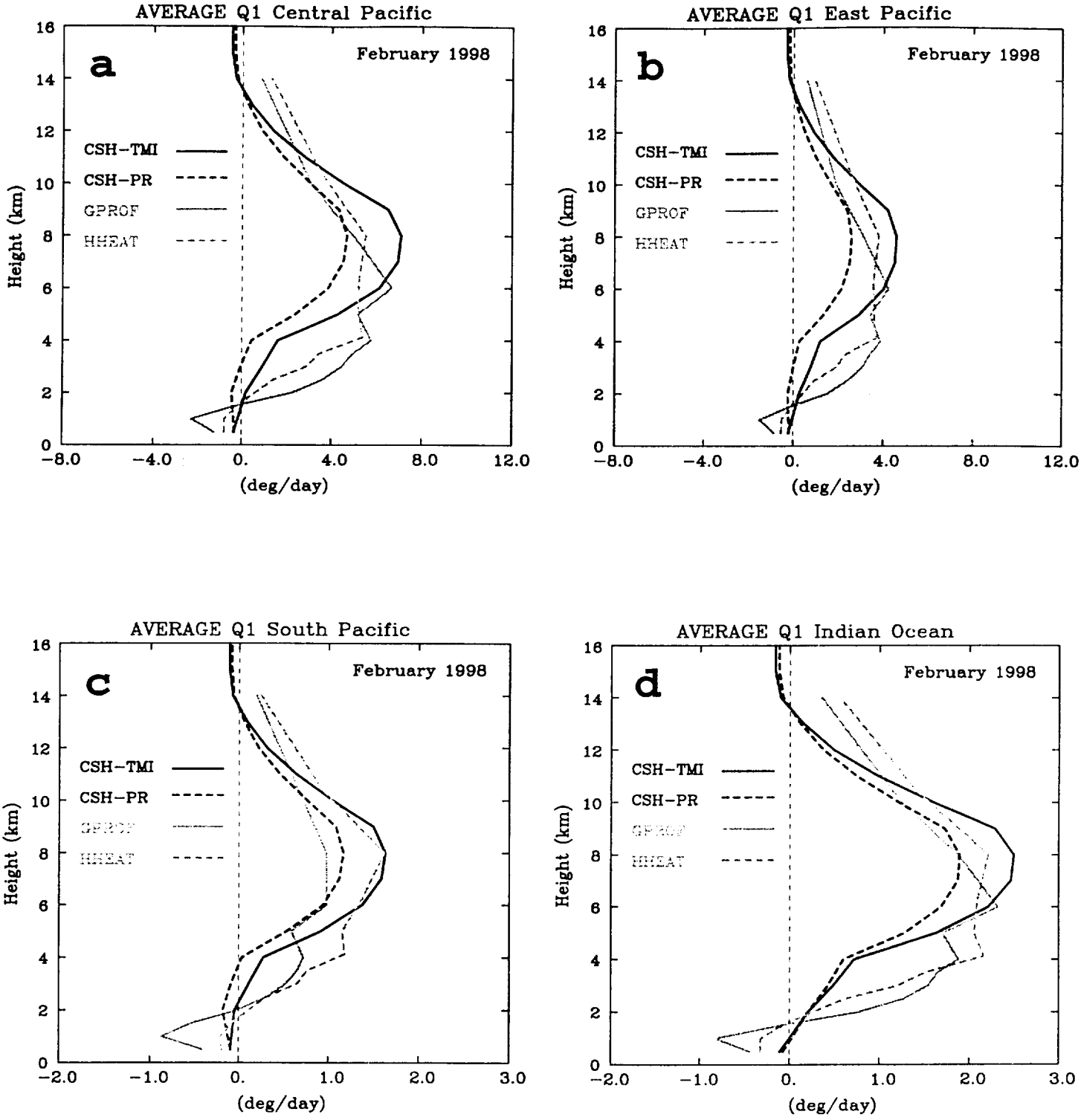
AVERAGE Q1 Central Pacific
a
February 1998
CSH-TMI
CSH-PR
GPROF
HHEAT
Height (km)
(deg/day)
AVERAGE Q1 East Pacific
b
February 1998
AVERAGE Q1 South Pacific
c
February 1998
AVERAGE Q1 Indian Ocean
d
February 1998

Fig. 11

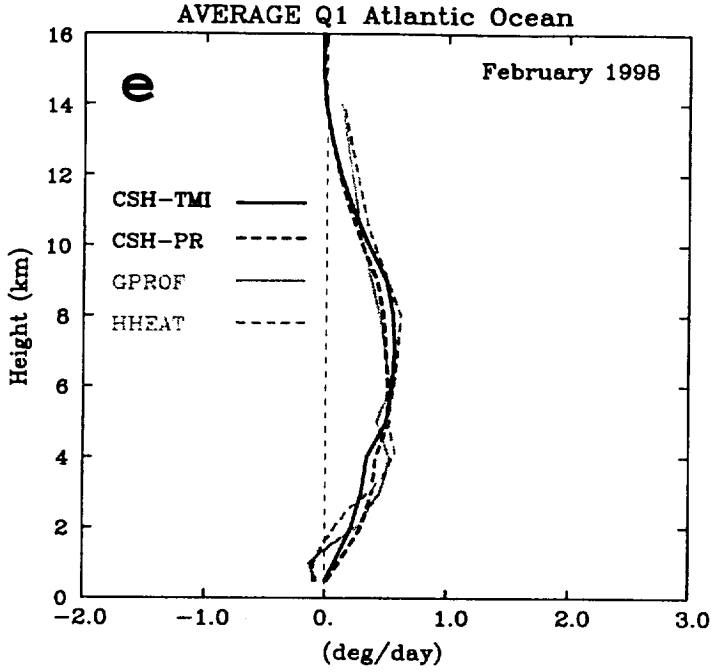
AVERAGE Q1 Atlantic Ocean
e
February 1998
CSH-TMI
CSH-PR
GPROF
HHEAT
Height (km)
(deg/day)

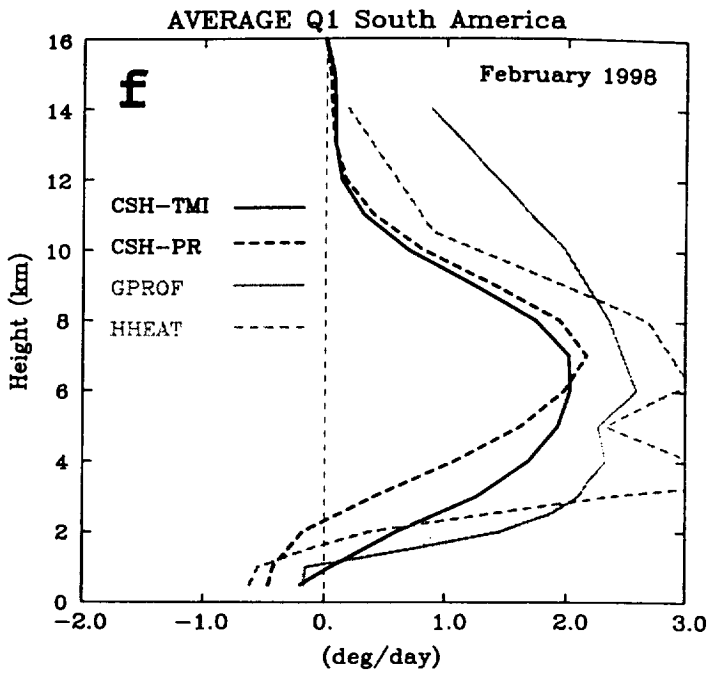
AVERAGE Q1 South America
f
February 1998
CSH-TMI
CSH-PR
GPROF
HHEAT
Height (km)
(deg/day)

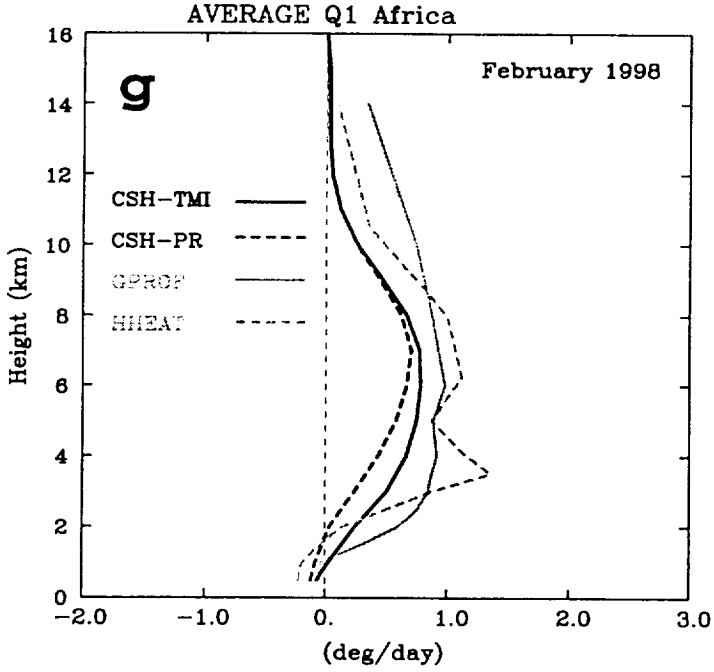
AVERAGE Q1 Africa
g
February 1998
CSH-TMI
CSH-PR
GPROF
HHEAT
Height (km)
(deg/day)

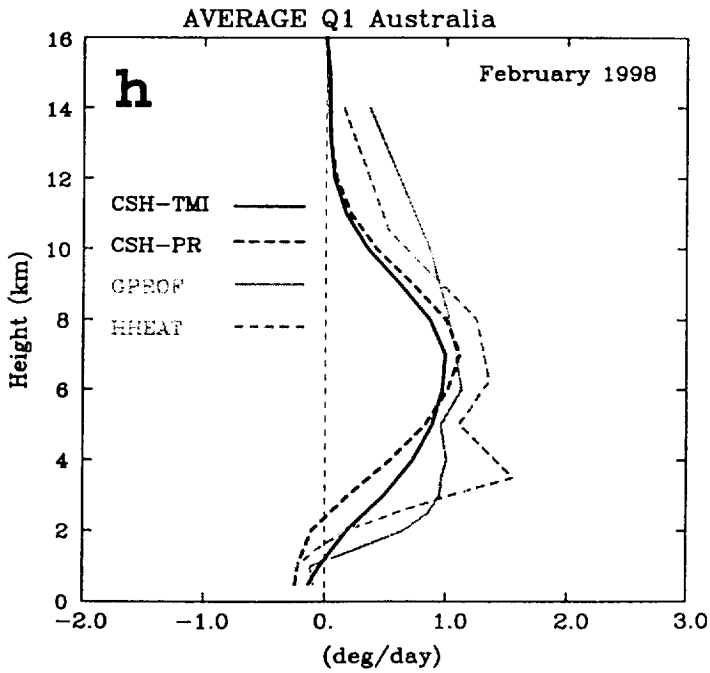
AVERAGE Q1 Australia
h
February 1998
CSH-TMI
CSH-PR
GPROF
HHEAT
Height (km)
(deg/day)

Fig. 11 (Cont)

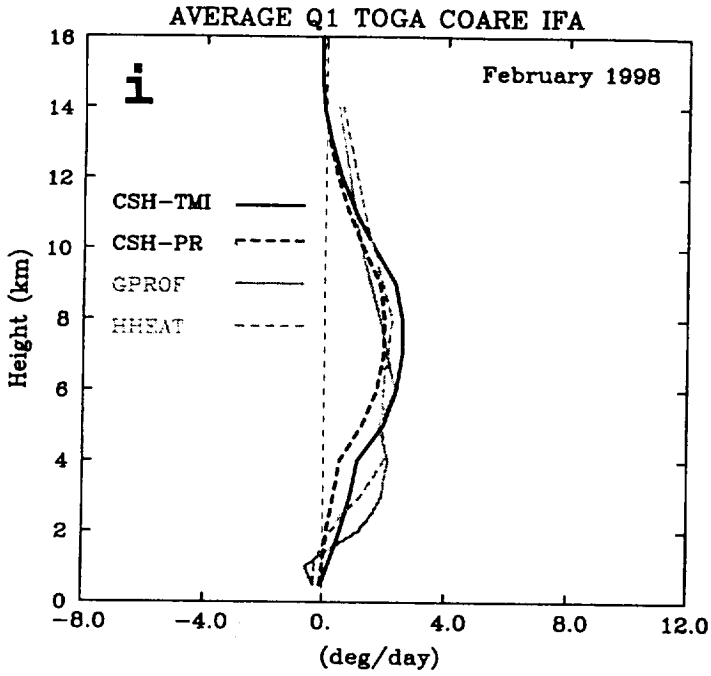
AVERAGE Q1 TOGA COARE IFA
i
February 1998
CSH-TMI
CSH-PR
GPROF
HHEAT
Height (km)
16
14
12
10
8
6
4
2
0
−8.0
−4.0
0.
4.0
8.0
12.0
(deg/day)

Fig. 11 (Cont)